NEUROSCIENCE

Synaptic-dependent developmental dysconnectivity in 22q11.2 deletion syndrome

Filomena Grazia Alvino[1]†, Silvia Gini[1,2]†, Antea Minetti[3], Marco Pagani[1,4], David Sastre-Yagüe[1,2], Noemi Barsotti[3,5], Elizabeth De Guzman[1], Charles Schleifer[6], Alexia Stuefer[1,2], Leila Kushan[6], Caterina Montani[1]‡, Alberto Galbusera[1], Francesco Papaleo[7,8], Wendy R. Kates[9], Declan Murphy[10,11], Michael Vincent Lombardo[12], Massimo Pasqualetti[1,3,5], Carrie E. Bearden[6,13]*†, Alessandro Gozzi[1]*†

Chromosome 22q11.2 deletion increases the risk of neuropsychiatric disorders like autism and schizophrenia. Disruption of large-scale functional connectivity in 22q11 deletion syndrome (22q11DS) has been widely reported, but the biological factors driving these changes remain unclear. We used a cross-species design to uncover the developmental trajectory and neural underpinnings of brain dysconnectivity in 22q11DS. In LgDel mice, a model for 22q11DS, we found age-specific patterns of brain dysconnectivity, with widespread fMRI hyperconnectivity in juvenile mice reconfiguring to hippocampal hypoconnectivity over puberty. These changes correlated with developmental alterations in dendritic spine density, and both were transiently normalized by GSK3β inhibition, suggesting a synaptic origin for this phenomenon. Notably, analogous pubertal hyperconnectivity-to-hypoconnectivity reconfiguration occurs in human 22q11DS, affecting cortical regions enriched for GSK3β-associated synaptic genes and autism-relevant transcripts. This dysconnectivity also predicts age-dependent social alterations in 22q11DS individuals. These results suggest that synaptic mechanisms underlie developmental brain dysconnectivity in 22q11DS.

INTRODUCTION

Complex developmental and neuropsychiatric disorders such as autism and schizophrenia have been consistently associated with dysfunctional interareal communication and atypical functional connectivity (*1*, *2*). These observations suggest that brain functional dysconnectivity (i.e., dysfunctional coupling between brain regions) is a system-level dimension that is key to the pathophysiology of these disorders (*3*–*5*). Computational and biophysical models support this view, showing that neuropsychiatric disorders can effectively be conceptualized as (functional) disconnection syndromes (*6*, *7*).

Despite the high prevalence of atypical functional connectivity in complex neuropsychiatric disorders, the specific underpinnings of these alterations remain poorly understood. Large-scale functional dysconnectivity may, in principle, reflect a combination of various multiscale contributing factors, ranging from anatomical miswiring (*8*, *9*) to functional and anatomical alterations in neural and synaptic coupling (*10*, *11*). However, the relative contribution of these components to specific brain disorders and their relationship to behavior have proven difficult to disambiguate. This problem is compounded by the highly heterogeneous etiology and manifestation of brain functional dysconnectivity across patient cohorts (*12*, *13*), which, together, have prevented a reliable decoding of imaging signals into physiologically interpretable events.

Investigations of brain dysconnectivity in genetically defined neuropsychiatric and developmental disorders may provide valuable mechanistic insight into the underpinnings of these alterations (*8*). A key benefit of this approach is the possibility of relating signatures of functional dysconnectivity to well-characterized etiological factors (and the biological cascade these trigger) in deeply phenotyped clinical populations. A second important benefit of this approach is the availability, for most of these prevalent syndromes, of animal models that can recapitulate clinically relevant mutations with high construct validity. Parallel investigations in human cohorts and physiologically accessible animal models can thus be used to generate testable hypotheses about the contribution (or lack thereof) of specific biological mechanisms to the establishment of brain dysconnectivity.

Chromosome 22q11.2 deletion is among the strongest known genetic risk factors for developmental disorders, including autism and schizophrenia (*14*, *15*). The relative high prevalence of 22q11.2 deletion syndrome (22q11DS), estimated to be ~1 per 3000 to 1 per 6000 live births in the general population (*16*, *17*), has prompted clinical and neuroimaging investigations in increasingly larger aggregated patient cohorts (*18*, *19*). Genomic and biological analyses of the ~46 genes that are typically affected by 22q11.2 deletion, and their modeling in rodents (*20*) have also provided initial clues about some of the putative biological processes underlying psychiatric risk in 22q11DS (*21*). Recapitulating findings in idiopathic autism and schizophrenia,

[1]Functional Neuroimaging Laboratory, Istituto Italiano di Tecnologia, Center for Neuroscience and Cognitive Systems @UniTn, Rovereto, Italy. [2]Center for Mind and Brain Sciences, University of Trento, Rovereto, Italy. [3]Department of Biology, Unit of Cell and Developmental Biology, University of Pisa, Pisa, Italy. [4]IMT School for Advanced Studies, Lucca, Italy. [5]Centro per l'Integrazione della Strumentazione Scientifica dell'Università di Pisa (CISUP), Pisa, Italy. [6]Department of Psychiatry and Biobehavioral Sciences, Semel Institute for Neuroscience and Human Behavior, University of California at Los Angeles, Los Angeles, CA, USA. [7]Genetics of Cognition Laboratory, Neuroscience Area, Istituto Italiano di Tecnologia, Genova, Italy. [8]IRCCS Ospedale Policlinico San Martino, Largo Rosanna Benzi, 10, 16132 Genova, Italy. [9]Department of Psychiatry and Behavioral Sciences, SUNY Upstate Medical University, Syracuse, NY, USA. [10]Department of Forensic and Neurodevelopmental Sciences, Institute of Psychiatry, Psychology and Neuroscience, King's College London, London, UK. [11]Institute of Translational Neurodevelopment, Institute of Psychiatry, Psychology and Neuroscience, King's College London, London, UK. [12]Laboratory for Autism and Neurodevelopmental Disorders, Center for Neuroscience and Cognitive Systems, Istituto Italiano di Tecnologia, Rovereto, Italy. [13]Department of Psychology, University of California at Los Angeles, Los Angeles, CA,USA.
*Corresponding author. Email: alessandro.gozzi@iit.it (A.G.); cbearden@mednet.ucla.edu (C.E.B.)
†These authors contributed equally to this work.
‡Present address: IRCCS Ospedale Policlinico San Martino, Genova, Italy.

brain imaging studies have revealed atypical patterns of functional connectivity in individuals with 22q11DS (*22*–*25*). However, the neural determinants and significance of the observed functional dysconnectivity remain undetermined. Moreover, the precise developmental trajectory of functional alterations in 22q11DS remains poorly understood. Because 22q11DS is associated with both early and late-onset neurodevelopmental disorders (*14*), gaining a better understanding of the developmental evolution of functional dysconnectivity in 22q11.2 deletion carriers may shed light on the relevance of this phenotype to 22q11DS pathology and specific symptom domains.

Recent progress in mouse brain imaging (*26*) offers the opportunity to generate and test mechanistic hypotheses about the underpinnings of brain dysconnectivity with great mechanistic precision (*11*). Leveraging cross-species neuroimaging data, here, we carried out a set of parallel studies in a mouse model of 22q11DS (*27*) and human 22q11.2 deletion carriers aimed to (i) track the developmental trajectory of functional dysconnectivity in this syndrome and (ii) probe the biological bases of these alterations. We find that 22q11DS dysconnectivity markedly reconfigures over puberty, where it mirrors co-occurring developmental alterations in dendritic spine density. We also show that this functional dysconnectivity is predictive of socio-behavioral alterations in 22q11.2 deletion carriers. These findings suggest that synaptic-related mechanisms underlie developmentally mediated functional dysconnectivity in 22q11DS.

RESULTS

fMRI dysconnectivity in LgDel mice reconfigures over puberty

To probe the developmental trajectory of functional dysconnectivity in 22q11DS, we conducted longitudinal resting-state functional magnetic resonance imaging (fMRI) connectivity mapping in LgDel mice, an established murine model of 22q11DS (*20*). By investigating fMRI connectivity in a rodent model, we sought to tightly control for environmental and genetic variability to a degree not feasible in human clinical research. Because 22q11DS is associated with both prepubertal and postpubertal neurodevelopmental disorders and given the profound developmental remodeling occurring during this critical time window, we carried out longitudinal fMRI connectivity mapping in LgDel mice before puberty [i.e., juvenile stage; (*28*)] and in young adulthood [i.e., postpubertal stage, postnatal day 35 ± 2 (PND35 ± 2) and PND111 ± 7, respectively; Fig. 1A]. To identify regional hubs or hotspots of fMRI dysconnectivity, we computed and compared at the voxel level maps of fMRI global connectivity (*29*), i.e., a measure of mean connectivity of each voxel with the rest of the brain.

Notably, this investigation highlighted robust alterations of fMRI connectivity in LgDel mice at both the developmental time points probed, with evidence of a developmental reconfiguration of the direction and anatomical location of these atypicalities over puberty (Fig. 1). Specifically, voxel-wise mapping of global fMRI connectivity revealed a transition from widespread hyperconnectivity in juvenile LgDel mice to more focal hypoconnectivity in adulthood. This hypoconnectivity primarily affected hippocampal regions and included also a regional cluster in the basal forebrain [Fig. 1B and fig. S1; $|t| > 2.0$, $P < 0.05$, family-wise error rate (FWER) cluster corrected; note that the right hippocampus (HPC) did not survive cluster correction; fig. S1]. Corroborating a developmental reconfiguration of fMRI dysconnectivity in LgDel mice, aggregate statistical modeling revealed significant age × genotype interaction in most of the affected regions (i.e., cortex and HPC; Fig. 1B, $|t| > 2.0$, $P < 0.05$, FWER cluster corrected).

Seed-based probing of known mouse connectivity networks (*30*) corroborated these findings. Specifically, we found that in juvenile LgDel mice the default-mode network (DMN) (fig. S2) was functionally hyperconnected to multiple basal forebrain regions (e.g., lateral septum and nucleus accumbens) (Fig. 1C). The same regions, however, exhibited fMRI hypoconnectivity (and a significant age × genotype interaction) in the same mice after puberty (Fig. 1C, $|t| > 2.0$, FWER cluster corrected). Similarly, seed-based probing of hippocampal regions did not reveal major connectivity alterations in juvenile LgDel mice but highlighted robust hypoconnectivity (and significant age × genotype interactions) with the anterior cingulate [a component of the mouse medial prefrontal cortex (PFC) (*31*) in adulthood; $|t| > 2.0$, FWER cluster corrected; Fig. 1D]. These effects (and their age × genotype interactions) were also apparent in subsequent quantifications of pairwise fMRI connectivity in regions of interest (Fig. 1, E and F). Collectively, these results reveal a previously unreported developmental reconfiguration of fMRI dysconnectivity over puberty in the LgDel model of 22q11DS.

Developmental dysconnectivity in 22q11.2 deletion carriers mirrors mouse findings

Prompted by our mouse findings, we next probed whether an analogous reconfiguration of fMRI dysconnectivity would also be identifiable over development in individuals with 22q11DS. To this purpose, we aggregated three independent fMRI datasets in 22q11DS [i.e., University of California Los Angeles (UCLA), King's College London (KCL), and SUNY Upstate Medical University (SUNY)], to obtain a single, harmonized cohort of $n = 139$ 22q11.2 deletion carriers (22q11DS) and $n = 117$ healthy controls (HCs), spanning an age range of 6 to 30 years old (Table 1 and table S1). To replicate the data analysis strategy that we used in the mouse, we split the clinical cohort into two age subgroups (Fig. 2A). Age ranges were chosen to broadly recapitulate corresponding developmental stage in rodents. We thereby defined a first age group that we herein refer to as childhood (age range, 6 to 11 years old; 22q11DS, $n = 21$; and HC, $n = 31$) and a second age group that we term postpuberty (age range, 12 to 30 years old; 22q11DS, $n = 118$; and HC, $n = 86$). We chose the age cutoff on the basis of previous work, pointing at age 11 being a peak of puberty onset [i.e., increased incidence of Tanner stages II/III; (*32*)].

As in our mouse investigations, we first carried out spatially unbiased global fMRI connectivity mapping in the two groups of participants (i.e., 22q11DS and HCs), at both ages. Paralleling our findings in LgDel mice, this analysis revealed a clear reconfiguration from hyper- to hypoconnectivity over puberty in people with 22q11DS (Fig. 2B). Specifically, in prepubertal 22q11 deletion carriers, we found extended foci of global fMRI hyperconnectivity in posterotemporal and somatomotor regions, as well as in the dorsal attention network. By contrast, postpubertal 22q11.2 deletion carriers exhibited robust fMRI hypoconnectivity relative to controls in the HPC and temporal lobe regions ($|t| > 2.0$, FWER cluster corrected). As seen in LgDel mice, most of the affected regions also exhibited robust age × genotype interactions ($|t| > 2.0$, FWER cluster corrected, Fig. 2B), thus supporting the notion of an altered developmental trajectory in 22q11DS. We observed the same developmental reconfiguration also upon excluding HC participants with mental health diagnoses and/or taking medication [spatial correlation Pearson's correlation coefficient (r) = 0.95,

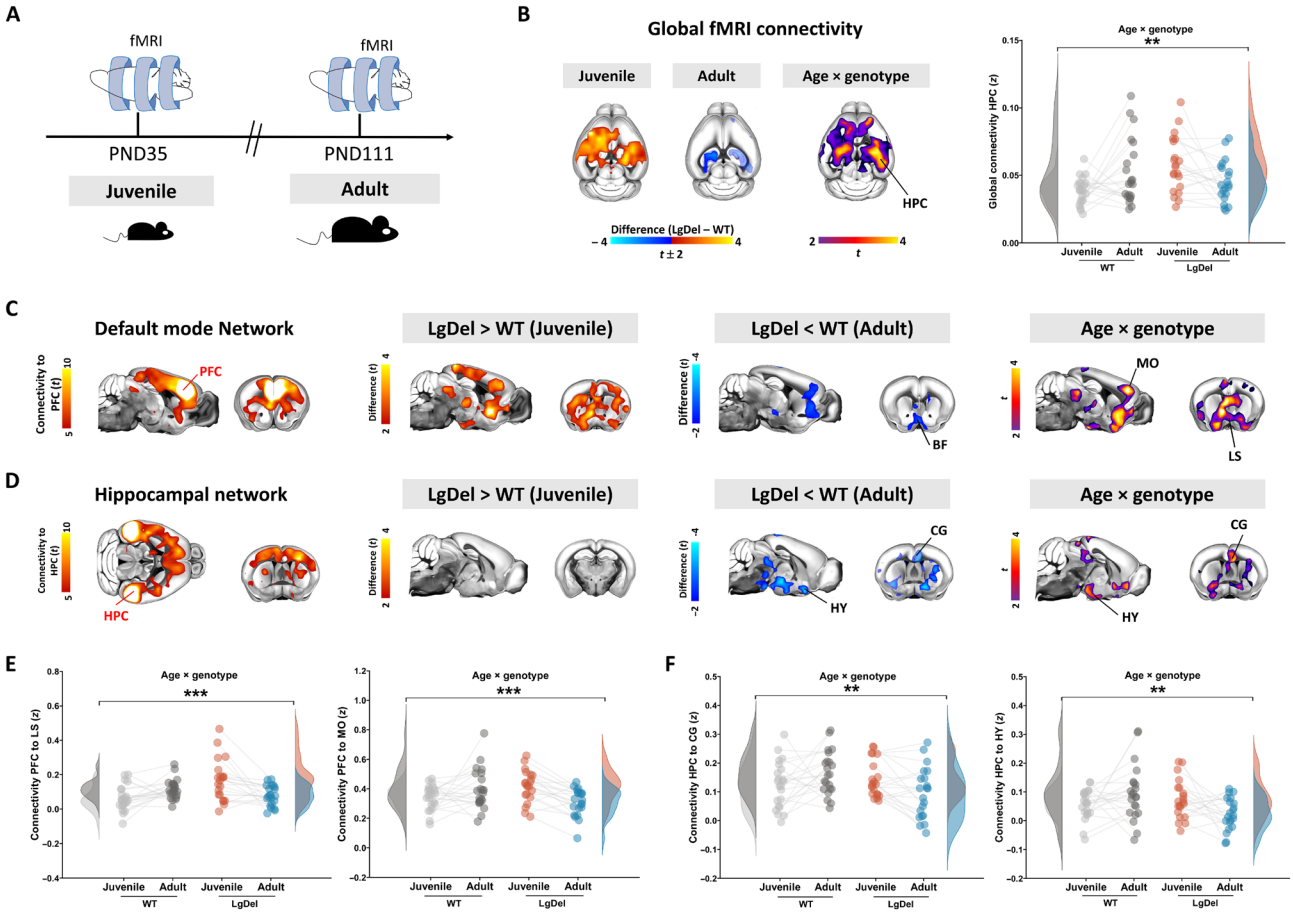

Fig. 1. Developmental fMRI dysconnectivity in LgDel mice. (**A**) Experimental timeline of fMRI mapping in wild-type (WT) and LgDel mice. (**B**) Whole-brain voxel-wise mapping of global fMRI connectivity revealed widespread hyperconnectivity in LgDel juvenile mice, reverting to focal hippocampal hypoconnectivity in the same animals after puberty. Maps are thresholded at $|t| > 2.0$, followed by family-wise error rate (FWER) correction at $P < 0.05$. Semitransparent right hippocampal blob indicates a cluster not surviving FWER correction (see fig. S1 for a comparison between uncorrected and corrected maps). Corresponding age × genotype maps and quantifications of fMRI global connectivity in dorsal hippocampal areas are reported for reference [two-way repeated-measures (RM) analysis of variance (ANOVA), age × genotype interaction, $F = 10.78$, $P = 0.0021$; WT, $n = 22$; and LgDel, $n = 21$]. (**C** and **D**) Seed-based mapping of the default-mode network (DMN) (C) and hippocampus (HPC) (D), respectively. Maps on the left show extension of reference DMN (C) and hippocampal (D) networks in juvenile WT mice. Corresponding between-group difference maps are reported for each of the probed developmental ages in the center panels. Red indicates increased fMRI connectivity, and blue indicates reduced fMRI connectivity compared to control WT littermates ($|t| > 2.0$, FWER corrected, $P < 0.05$). (**E** and **F**) Regional quantification of pairwise fMRI connectivity between regions of the DMN (E) and hippocampal networks (F) exhibiting significant age × genotype interaction (two-way RM ANOVA, DMN: $F = 15.48$, $P = 0.0003$, and $F = 14.72$, $P = 0.0004$; HPC: $F = 8.67$, $P = 0.0053$, and $F = 7.36$, P = 0.0097) as per maps in (C) and (D). Each point represents a mouse. $^{**}P < 0.01$, and $^{***}P < 0.001$. BF, basal forebrain; CG, cingulate cortex; HY, hypothalamus; LS, lateral septum; MO, motor cortex; PFC, prefrontal cortex.

$P < 0.0001$; fig. S3, A and B] or by restricting postpubertal group to only include individuals aged 18 to 30 ($n = 49$ HCs and $n = 82$ 22q11DS, age × genotype interaction, spatial correlation Pearson's $r = 0.95$, $P < 0.0001$; fig. S3C). Last, an additional analysis within one site only (UCLA specifically) confirmed the presence of a developmental dysconnectivity reconfiguration analogous to that observed in the original sample reported in Fig. 2B (fig. S4; spatial correlation Pearson's $r = 0.84$, $P < 0.0001$), thus suggesting that our results are not driven by site differences.

To probe the brain networks most affected by these alterations, we conducted a targeted seed-based analysis of the regional clusters that exhibited a statistically significant age × genotype interaction in our global connectivity mapping (seed location in fig. S5). Seed probing of a cluster located in the right opercular cortex [a component of the somatomotor/auditory network; (*33*)] showed that prepubertal individuals with 22q11DS exhibited an aberrant extension of this network extending beyond somatomotor regions to include regions belonging to the DMN (middle frontal gyrus, cingulate gyrus, and precuneus) and dorsal attention network (lateral occipital cortex; Fig. 2C). After puberty, the same network appeared to be largely hypoconnected in 22q11DS. Notably, analogous findings were obtained when probing fMRI connectivity of an age × genotype interaction cluster located in the postcentral gyrus (fig. S6A). We also conducted seed-based probing of the HPC (Fig. 2D) to test whether postpubertal 22q11DS carriers would exhibit hypoconnectivity of this region, as found in mice. This analysis showed that focal hippocampal dysconnectivity in prepubertal 22q11.2 deletion carriers evolves into robust and widespread hypoconnectivity after puberty. Mirroring mouse findings, the medial PFC was among the regions exhibiting a transition from hyperconnectivity to hypoconnectivity (i.e., a significant age ×

Table 1. Demographic and clinical information for participants included in the study. ASD, autism spectrum disorder; ADHD, attention-deficit hyperactivity disorder; M, male; F, female. *$P < 0.05$, **$P < 0.01$, and ***$P < 0.001$; 22q11DS versus HC; Student's *t* test or Fisher's exact test.

	Children (6 to 11 years)		Postpubertal (12 to 30 years)	
	HC ($n = 31$)	22q11DS ($n = 21$)	HC ($n = 86$)	22q11DS ($n = 118$)
Age (years)	8.85 ± 2	9.4 ± 2	18.4 ± 4	19.4 ± 4
Sex (M/F)	15/16	9/12	41/45	54/64
Full-scale IQ† (means ± SD)	117.3 ± 22.6	77.7 ± 7.2***	109.4 ± 16.4	79.9 ± 13.9***
ASD, *n* (%)	0 (0)	7 (33)***	0 (0)	16 (13.5)***
ADHD, *n* (%)	1 (3)	10 (48)***	7 (8)	36 (30)***
Psychotic disorder, *n* (%)	0 (0)	0 (0)	0 (0)	7 (5.9)*
Anxiety disorder, *n* (%)	1 (3)	7 (33)**	10 (12)	30 (25)*
Mood disorder, *n* (%)	0 (0)	2 (9.5)	4(5)	29 (25)***
Current antipsychotic treatment, *n* (%)	0 (0)	1 (3)	0 (0)	14 (12)***
Current antidepressant/antianxiety treatment, *n* (%)	0 (0)	0 (0)	2 (2.3)	24 (20)***
Current psychostimulant treatment, *n* (%)	1 (3)	1 (3)	3 (3.5)	13 (11)*

†Intelligence quotient (IQ) data were not available for $N = 1$ child HC, $N = 2$ children 22q11DS, $N = 9$ postpubertal HC, and $N = 2$ postpubertal 22q11DS.

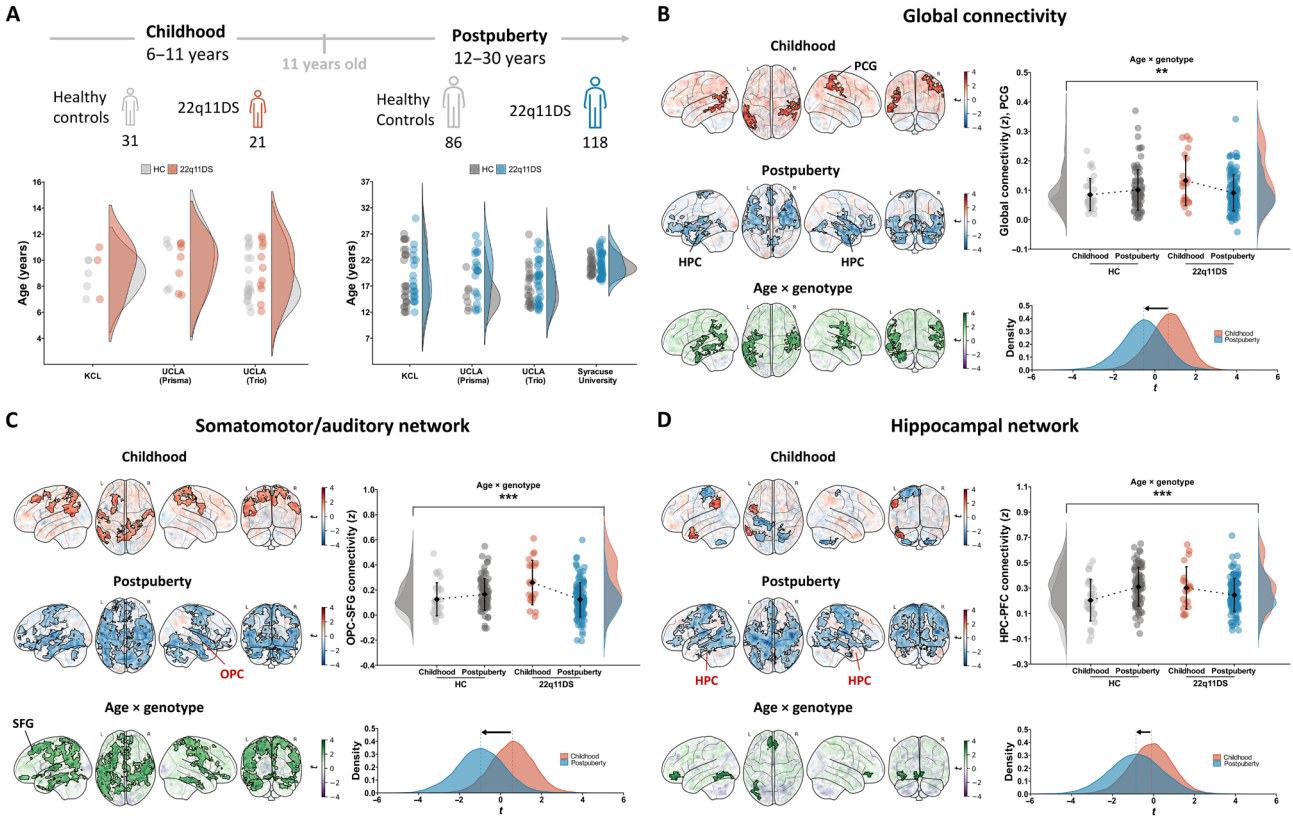

Fig. 2. Developmental fMRI dysconnectivity in human 22q11DS. (**A**) Schematic representation of human cohort divided into the childhood cohort (HC, $n = 31$; and 22q11DS, $n = 21$) and the postpubertal cohort (HC, $n = 86$; and 22q11DS, $n = 118$). Distribution of age for each diagnosis (HC and 22q11DS) across sites and scanners. (**B**) Voxel-wise (left) mapping of global fMRI connectivity revealed increased functional connectivity in 22q11DS carriers during childhood and reduced fMRI connectivity in the postpubertal cohort. Semitransparent maps in the background represent unthresholded *t* values. Clusters surviving FWER correction are outlined in black. Areas exhibiting a significant age × genotype interaction were identified using a linear model (two-way ANOVA, age × genotype interaction, $F = 7.87$, $P = 0.0054$). Whole-brain distribution of *t* values resulting from group differences at each age revealed a robust shift (arrow) from prevalent hyperconnectivity in childhood to prevalent hypoconnectivity after puberty (bottom right). (**C** and **D**) Seed-based analysis using clusters exhibiting significant age × genotype interaction in our global fMRI connectivity analysis as seeds: OPC (two-way ANOVA, $F = 16.72$, $P < 0.0001$) (C) and HPC (two-way ANOVA, $F = 12.36$, $P = 0.0005$) (D). Distribution of *t* values resulting from between-group connectivity differences over development are also reported for reference. Note shift from hyper- to hypoconnectivity (arrow) occurring over puberty. **$P < 0.01$, and ***$P < 0.001$. SFG, superior frontal gyrus.

genotype interaction, $|t| > 2.0$, FWER cluster corrected) during development (Fig. 2D and fig. S6B).

Last, we assessed whether considering age as a continuous variable would reveal a trajectory of developmental dysconnectivity broadly consistent with our a priori categorical analysis of prepubertal and postpubertal cohorts. We thus used a nonlinear mixed model [general additive mixed model (GAMM); (*34*)] to probe the relationship between age and fMRI global connectivity in cortical regions undergoing developmental reconfigurations within the somatomotor/auditory network (i.e., opercular cortex, and postcentral gyrus) and in the HPC. We found the corresponding trajectories of dysconnectivity to be broadly consistent with our age cutoff. Specifically, hyperconnectivity persisted until age 9.2 and 9.9 years in opercular cortex and postcentral gyrus, respectively. Reversal to hypoconnectivity was observed in opercular regions at age of 13.8 years. In the HPC, we found the onset of hypoconnectivity to occur at age 12.8 years (fig. S7). These results support our use of a cutoff developmental point of 11 years of age. More broadly, our investigations document the presence of developmental fMRI dysconnectivity in 22q11DS, involving a transition from hyperconnectivity to hypoconnectivity relative to typically developing controls across puberty.

GSK3β-dependent synaptic alterations underlie developmental dysconnectivity in LgDel mice

The observed correspondence between human and mouse neuroimaging findings prompted us to use the LgDel model to investigate the neurobiological underpinnings of developmental fMRI dysconnectivity in 22q11DS. Neuroanatomical investigations have provided evidence of synaptic-related pathology and altered dendritic spine density in LgDel mice and other rodent models of 22q11DS, especially in hippocampal areas (*35*–*37*). Using in vivo manipulations and computational modeling, we recently showed that alterations in dendritic spine density can be putatively mirrored by corresponding changes in global fMRI connectivity, with increased or decreased spine density being paralleled by increased (*10*) and decreased (*38*) global fMRI connectivity, respectively. These observations suggest that synaptic-related mechanisms might contribute to fMRI dysconnectivity in LgDel mice. This hypothesis would be consistent with the profound synaptic remodeling occurring in the mammalian brain during adolescence (*39*).

To test this hypothesis, we first measured dendritic spine density in the PFC and HPC of LgDel mice at juvenile and adult stage (Fig. 3A and fig. S8). We found that dendritic synaptic density was altered in both the probed regions, albeit with different developmental trajectories. Specifically, spine density in the PFC was robustly increased in juvenile LgDel mice but showed highly comparable values between groups in adulthood [Fig. 3A; $P < 0.0001$ and $P > 0.99$, respectively, Sidak's multiple comparisons test, two-way analysis of variance (ANOVA); fig. S8]. In the HPC, we found a similar increase in dendritic spine density in juvenile LgDel animals. However, a reversed phenotype was observed after puberty, with LgDel mice exhibiting significantly lower spine density than WT littermates (Fig. 3A; $P < 0.0001$ and $P = 0.01$, respectively, Sidak's multiple comparisons test, two-way ANOVA; fig. S8).

To putatively link alterations in spine density to the observed fMRI dysconnectivity, we next quantified global fMRI connectivity in PFC and HPC and compared the observed fMRI connectivity differences with the corresponding alterations in spine density (Fig. 3B). Global fMRI connectivity quantifications broadly recapitulated the group- and age-specific profile observed in dendritic spine count experiments. Specifically, fMRI connectivity was only transiently increased in the PFC of LgDel mice at the juvenile stage, while juvenile fMRI hyperconnectivity in the HPC fully reverted to hypoconnectivity in adulthood. Moreover, intergroup differences in global fMRI connectivity and spine density were found to covary (Fig. 3C). These findings suggest that developmental hyper- and hypoconnectivity in LgDel mice might reflect increased and decreased synaptic density, respectively.

If alterations in synaptic density are causally implicated in the fMRI dysconnectivity that we observed in LgDel mice, then normalization of synaptic pathology should be associated with a normalization of fMRI phenotypes. To test this hypothesis, we leveraged previous reports that the glycogen synthase kinase-3 β (GSK3β) pathway is hyperactive in rodent models of 22q11DS (*40*). GSK3β is a critical regulator of synaptic development and function (*40*–*42*). GSK3β overactivity may thus lead to impaired synaptic homeostasis and interfere with the large-scale synaptic pruning and refinement that occurs during childhood and adolescence, resulting in altered dendritic spine density.

To test the hypothesis that GSK3β hyperactivity may underlie synaptic alterations observed in LgDel mice, we pharmacologically inhibited GSK3β via administration of the selective antagonist SB216763 (SB) during the first three postnatal weeks (Fig. 3D). This developmental period is characterized by robust spine growth and synaptogenesis, as well as high expression of GSK3β (*42*, *43*). We next measured dendritic spine density in the PFC and whole-brain fMRI connectivity in two separate groups of mice (Fig. 3E and fig. S8).

Because SB was administered during an early developmental window, we expected this treatment to be able to (at least transiently) normalize the synaptic and fMRI connectivity alterations that we found in juvenile mice. Corroborating this notion, developmental GSK3β inhibition significantly reduced spine density surplus in the PFC of juvenile LgDel mice (Fig. 3E, two-way ANOVA, Sidak's multiple comparisons test, LgDel SB versus LgDel VEH, $P = 0.01$; fig. S8). This treatment also robustly normalized fMRI hyperconnectivity in mice imaged at the same prepubertal stage, as probed either with global fMRI mapping or seed-based mapping of the DMN (two-way ANOVA, Sidak's multiple comparisons test, LgDel SB versus LgDel VEH, $P = 0.0009$, Fig. 3E and fig. S9). Corroborating a possible link between synaptic alterations and fMRI dysconnectivity, dendritic spine density and global fMRI connectivity were found to be unaltered in the PFC of adult mice receiving SB or vehicle (VEH) administration (figs. S8 and S10). Similar concordant changes in spine density and fMRI connectivity were observed across ages in the HPC (fig. S10C). Together, these results implicate GSK3β-dependent synaptic alterations in the establishment of developmental fMRI dysconnectivity that we identified in LgDel mice. The observed normalization of fMRI dysconnectivity was transient and did not extend to adulthood (fig. S10B), as we found that foci of global hippocampal fMRI hypoconnectivity in adult LgDel were not affected by postnatal pharmacological treatment with SB (fig. S10D).

To probe the behavioral relevance of these connectivity alterations, we next assessed social behavior and cognitive function in juvenile and adult mice, with and without treatment with SB. These investigations highlighted the presence of translationally relevant behavioral alterations in LgDel mice. At the juvenile stage, LgDel mice displayed impaired sociability in a social habituation-dishabituation

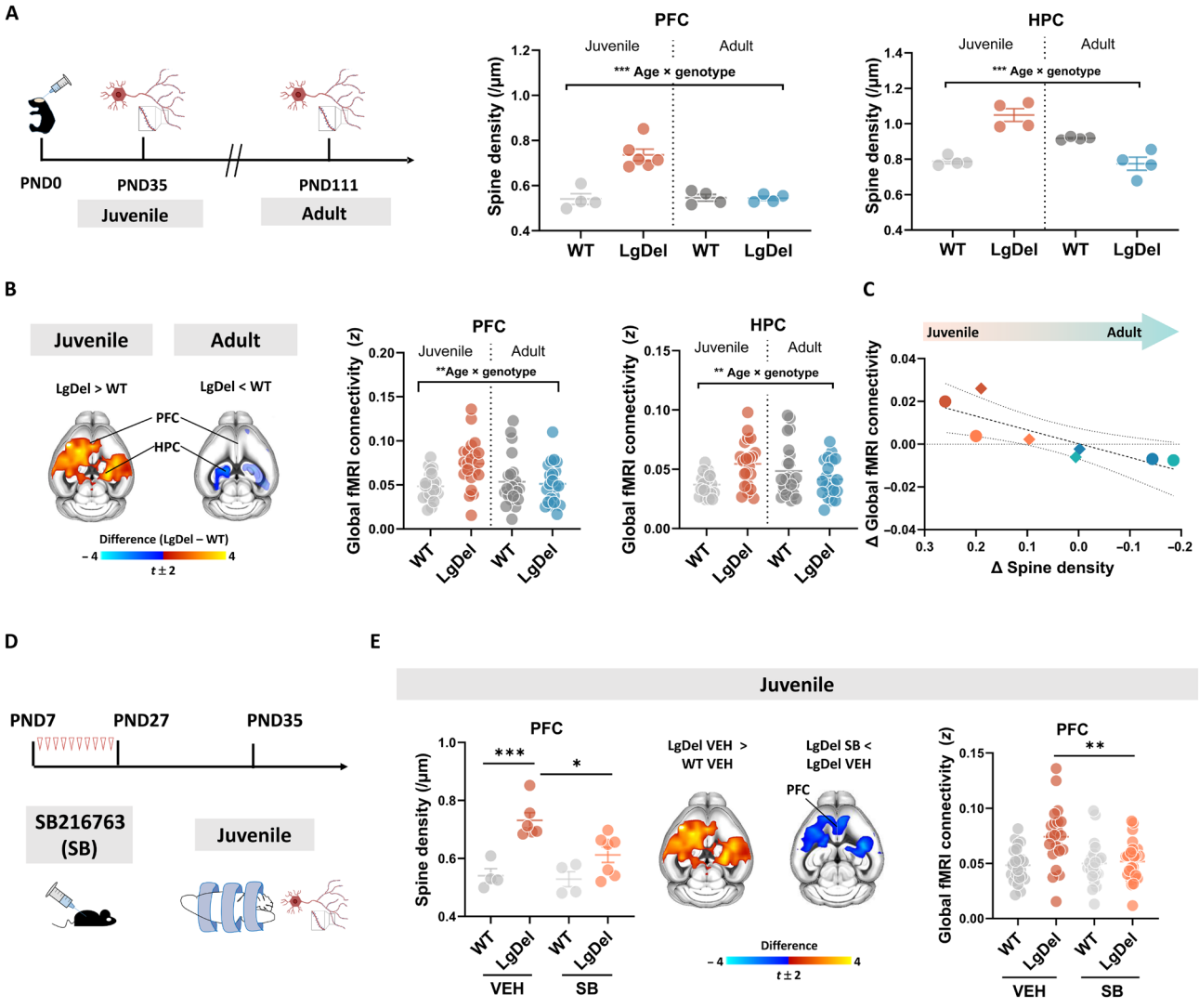

Fig. 3. Developmental fMRI dysconnectivity is paralleled by GSK3β-dependent alterations in dendritic spine density. (**A**) Dendritic spine density measurements across development in the PFC and the HPC revealed a significant age × genotype interaction (two-way ANOVA, age × genotype interaction; PFC: $F = 19.86$, $P = 0.0005$; HPC: $F = 58.28$, $P < 0.0001$). (**B**) Voxel-wise global fMRI connectivity in these two areas exhibited a similar developmental trajectory, with a significant age × genotype interaction both in PFC and HPC (two-way RM ANOVA, age × genotype interaction; PFC: $F = 8.8$, $P = 0.005$; and HPC: $F = 10.42$, $P = 0.0025$). Each point represents a different mouse. (**C**) Intergroup differences in synaptic density and fMRI global connectivity show a linear relationship [coefficient of determination (R^2) = 0.68; P = 0.01]. Color of the dots represents group [red, juvenile vehicle (VEH); orange, juvenile SB treated; dark blue, adult VEH; green, adult SB treated], while shape represents region (circle, HPC; diamond, PFC). This plot includes data from (C) and fig. S10. (**D**) Experimental timeline of the GSK3β inhibition treatment protocol (from PND7 to PND27), followed by fMRI and spine density measurements. (**E**) Developmental GSK3β inhibition rescued spine density increase in PFC of juvenile mice (two-way ANOVA, Sidak's multiple comparisons test, LgDel SB versus LgDel VEH, $P = 0.01$). Similarly, the same treatment restored global fMRI connectivity alterations in juvenile LgDel mice (two-way ANOVA, Sidak's multiple comparisons test, LgDel SB versus LgDel VEH, $P = 0.0009$). Maps are thresholded at $|t| > 2.0$, followed by FWER correction at $P < 0.05$. Errors bars represents SEM. $^*P < 0.05$, $^{**}P < 0.01$, and $^{***}P < 0.001$.

test (two-way ANOVA, LgDel VEH versus WT VEH, $P = 0.04$; fig. S11). However, these impairments were unchanged by GSK3β inhibition (LgDel SB versus LgDel VEH, $P = 0.07$). Juvenile LgDel mice did not show overt alterations in social reward processing, as probed with a social conditioned place preference (SCPP) task (LgDel VEH versus WT VEH, $P = 0.26$; fig. S11). This behavior was also not affected by GSK3β treatment (LgDel SB versus LgDel VEH, $P = 0.97$).

Similar to what was observed at the juvenile stage, adult LgDel mice displayed reduced sociability (two-way ANOVA, LgDel VEH versus WT VEH, $P = 0.047$) but broadly preserved social memory (LgDel VEH versus WT VEH, $P = 0.18$; fig. S11) in a three-chamber social approach task. Pharmacological GSK3β inhibition did not mitigate these socio-behavioral alterations. Last, adult LgDel mice exhibited impaired cognition in a temporal-order memory task (two-way ANOVA, LgDel VEH versus WT VEH, $P = 0.002$). In contrast to the other paradigms, this deficit was ameliorated by GSK3β inhibition (LgDel SB versus LgDel VEH, $P = 0.003$; fig. S11). Together, these investigations provide evidence of social alterations and impaired memory–related cognition in adult LgDel mice, with only the latter being improved by GSK3β inhibition. These observations also

suggest that, while modulating GSK3β activity may reestablish (synaptic and fMRI) brain connectivity and memory-related cognition in LgDel mice, this pathway may be less implicated in the control of social behavior.

To more rigorously probe the relationship between behavioral alterations and fMRI dysconnectivity in LgDel mice, we used partial least squares analysis (*44*) to model covariance between fMRI connectivity and behavioral performance in the tests described above. By using a multivariate approach, we sought to control for statistical bias related to repeated univariate testing of multiple behavior (*45*). This "brain-behavior" relationship was assessed for connectivity in the DMN and hippocampal networks, i.e., two systems encompassing key substrates for social and memory-related functions (*10*, *46*, *47*). We also assessed possible modulation by GSK3β-inhibition of brain-behavioral covariance patterns by entering treatment as a binary design variable in the behavioral matrix.

In line with previous reports (*10*, *47*), we found, both in juvenile and adult wild-type (WT) mice, significant covariance between sociability and fMRI connectivity in striatocortical components of the DMN (fig. S12). In LgDel mice, this relationship was disrupted, such that neither prefrontal nor hippocampal patterns of connectivity were found to covary with behavioral profiles in the same fashion as WT mice (fig. S12). The lack of significant covariance between treatment and behavioral performance further suggested that the brain-behavior relationship was not restored by pharmacological GSK3β inhibition. These results suggest that connectivity-behavior relationships are disrupted in LgDel mice and that this relationship is not restored by developmental treatment with SB.

Developmental dysconnectivity affects regions enriched for GSK3β-interacting synaptic genes

Our mouse investigations suggest that synaptic-related mechanisms and, specifically, GSK3β pathway dysregulation may underlie fMRI dysconnectivity in LgDel mice. To probe the generalizability of these findings to human 22q11DS, we used a gene decoding approach to relate the observed developmental dysconnectivity to spatial patterns of postmortem gene expression in the same regions (*48*). We thus identified a list of $N = 3897$ transcripts (henceforth "decoded genes") that are spatially enriched in areas exhibiting developmental dysconnectivity in individuals with 22q11DS (Fig. 4A). We next ran an enrichment analysis for genes implicated in synaptic signaling as defined by gene ontology (GO) categories (*49*). In keeping with our hypothesis, we found a significant enrichment for multiple synaptic-related GO gene lists, with odds ratio (OR) well above those observed in the spatial autocorrelation preserving null distribution (Fig. 4B). This result suggests that these enrichments are anatomically specific to regions undergoing developmental reconfiguration during puberty. No enrichment for glial-, microglia-, or immune-related genes was observed (table S2).

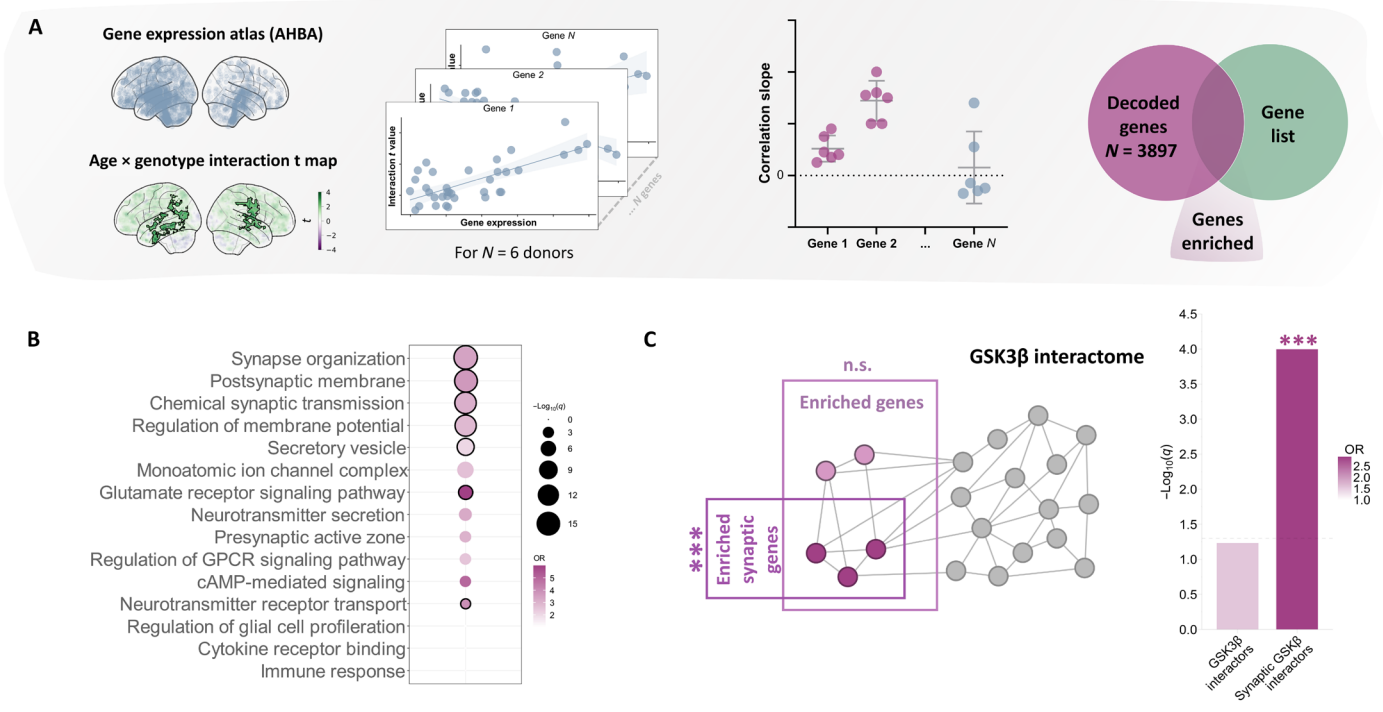

Fig. 4. Gene decoding supports involvement of synaptic mechanisms in 22q11DS developmental dysconnectivity. (**A**) Illustration of gene decoding and gene enrichment analyses used to investigate molecular mechanisms underlying developmental reconfiguration. The term "decoded genes" refers to genes that were spatially enriched (i.e., genes that displayed significantly higher expression) in areas that undergo hyperconnectivity-to-hypoconnectivity reconfiguration in 22q11DS. (**B**) Decoded genes are specifically and significantly enriched for synaptic-related gene ontology (GO) gene lists, corroborating the involvement of synaptic mechanisms in 22q11DS dysconnectivity. Color scale indicates OR, while size of the dots represents $-\log_{10}(q \text{ value})$. Only visible dots were statistically significant at $q < 0.05$. Black outlines around dots represent observed OR above 95th percentile of null distribution. cAMP, cyclic adenosine 3′,5′-monophosphate; GPCR, G protein–coupled receptor. (**C**) Schematic representation of gene enrichment analyses (left) and results (right) showing significant enrichment for synaptic interactors of GSK3β (hypergeometric test, OR = 2.91, $q = 0.0002$, overlapping genes, $N = 45$). Bar color indicates OR, length represents $-\log_{10}(q \text{ value})$. Horizontal dashed line (in gray) represents significance at $q < 0.05$. ***$P < 0.001$. n.s., not significant.

To corroborate putative mechanistic correspondences with our mouse data, we next investigated whether brain regions undergoing developmental dysconnectivity in individuals with 22q11DS would be specifically enriched for GSK3β -related synaptic genes. To test this hypothesis, we first examined whether the decoded genes would be enriched for genes that interact at the protein level with GSK3β. This analysis revealed a weak enrichment of GSK3β interactors in the decoded gene list (OR = 1.57; $q = 0.06$; overlapping genes, $N = 129$; Fig. 4C). However, when we pruned this list to solely retain GSK3β interactors involved in synaptic processes as per the curated SYNGO database (*50*), we found the decoded list to be robustly enriched for these transcripts (OR = 2.91; $q = 0.0001$; overlapping genes, $N = 45$; Fig. 4C and table S2). To test the spatial specificity of this result, we applied gene decoding on $k = 1000$ spatial autocorrelation-preserving surrogate maps. Enrichment analyses of the gene lists decoded from these surrogates suggest that our enrichment was unique to our developmental dysconnectivity pattern, as the OR of our enrichment mapped above 99th percentile of the obtained null distribution. These results suggest that GSK3β-related synaptic mechanisms may also underlie developmental dysconnectivity in human 22q11DS dysconnectivity.

The lack of a complete rescue effect following GSK3β inhibition raises the possibility that other pathways might be involved in the establishment of postpubertal hypoconnectivity. To explore this possibility, we probed whether our brain-decoded genes would be enriched for additional synaptic pathways. To this aim, we identified, within the 22q11.2 deletion locus, genes that are (i) involved in synaptic function as per the SYNGO database (*50*) and (ii) deleted in the LgDel mouse model. Four genes within the 22q11.2 locus met these criteria: COMT, DGCR8, RNT4R, and SEPT5 (termed here 22q11SG). We found that areas exhibiting fMRI dysconnectivity in 22q11DS were significantly enriched with synaptic-related transcripts directly interacting with 22q11SG (OR = 2.73; $q = 0.0002$; overlapping genes, $N = 48$; fig. S13A). We note here that this enrichment did not survive correction for the contribution of spatial autocorrelation at a percentile threshold of 95%. However, we found significant overlap between the genes enriched in the GSK3β synaptic interactome and those enriched in the synaptic interactome obtained using 22q11SG (OR = 8.98, $P = 0.000004$; fig. S13B). This finding suggests that these two synaptic pathways may intersect and potentially converge to contribute to 22q11DS functional dysconnectivity.

Developmental dysconnectivity within sensory-motor systems predicts social impairment in 22q11DS

To investigate the potential clinical relevance of the observed developmental dysconnectivity in 22q11DS, we probed whether the decoded gene list would be significantly enriched for subcategories of genes known to be involved in neurodevelopmental disorders. We found that the pattern of developmental dysconnectivity that we identified in 22q11DS individuals (Fig. 2B) was spatially enriched for genes involved in schizophrenia and for genes associated with autism. However, enrichment for autism-relevant gene lists, especially genes whose expression is reduced in postmortem cortical samples of autistic people, was stronger and exhibited especially high significance [(*51*): OR = 4.15; $q < 0.0001$; overlapping genes, $N = 917$; Simons Foundation Autism Research Initiative gene list: OR = 2.08; $q < 0.0001$; overlapping genes, $N = 334$; Fig. 5A). The observed ORs for all of these lists were above the 95th percentile of null ORs obtained from spatial autocorrelation-preserving null maps. No enrichment for genes associated with bipolar disorder (*52*) or attention-deficit hyperactivity disorder (ADHD) (*53*) was found (Fig. 5A and table S3).

The observation of a disproportionately high enrichment for genes exhibiting functional down-regulation in autism (Fig. 5A; $P = 10^{-113}$) led us to hypothesize that the observed developmental dysconnectivity may be associated with autism-relevant symptoms in people with 22q11DS. Such notion would be consistent with the prepubertal manifestation of hyperconnectivity in 22q11DS individuals. We thus selected a subset of $N = 129$ 22q11.2 deletion carriers ($N = 18$ children and $N = 111$ adults) for which we had corresponding social responsiveness scale (SRS) scores and used a linear model to test the hypothesis that magnitude of fMRI dysconnectivity in areas undergoing the developmental switch (i.e., those showing significant age × genotype interaction) would be predictive of reciprocal social behavior impairment, assessed via SRS score. If this is the case, then SRS scores in 22q11DS individuals would be positively associated with fMRI hyperconnectivity in childhood and negatively associated with fMRI hypoconnectivity in adulthood, respectively. The application of this model

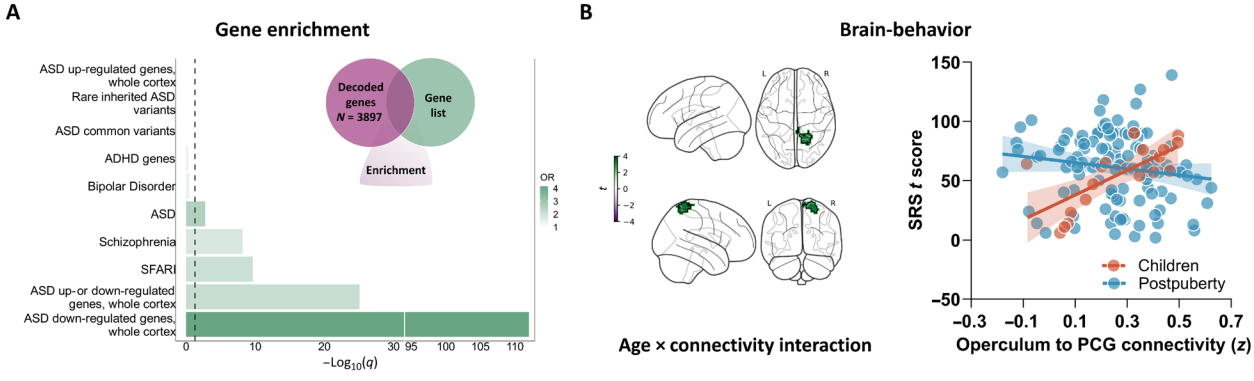

Fig. 5. Developmental fMRI dysconnectivity within somatomotor areas correlates with reciprocal social behavior in 22q11DS. (**A**) Gene enrichment analyses showing highly significant enrichment between decoded genes and schizophrenia- and autism spectrum disorder (ASD)–related genes. Bar color indicates OR, and length represents $-\log_{10}(q$ value). Vertical dashed line (in gray) represents significance at $q < 0.05$. (**B**) Voxel-wise (left) and region of interest–based quantifications of relationship between opercular cortex connectivity and SRS score in 22q11 deletion carriers. Map represents areas of significant correlation between the age × connectivity interaction and SRS score ($|t| > 2.0$, FWER cluster corrected). Visualization of relationship between opercular cortex to postcentral gyrus (PCG) connectivity and SRS within the two age groups separately (right).

to fMRI global connectivity maps did not reveal such an association ($P > 0.05$, FWER cluster corrected). However, global fMRI connectivity is an aggregate voxel-wise measure that incorporates multiple, potentially contrasting network-specific associations. We thus applied our model to the fMRI connectivity maps obtained via seed-based mapping of the postcentral gyrus and opercular cortex. While no significant association was detected for postcentral gyrus seed-based maps ($P > 0.05$, FWER cluster corrected), linear modeling of the somatomotor/auditory network connectivity revealed a cortical cluster exhibiting a significant developmental interaction between SRS and fMRI connectivity (age × fMRI connectivity, $|t| > 2.0$, FWER cluster corrected; Fig. 5B). As hypothesized, this relationship was characterized by a positive association between fMRI connectivity and SRS in childhood, which reverted to a negative association after puberty (Fig. 5B, rightmost panel). These results suggest that the hyperconnectivity-to-hypoconnectivity switch in sensory-motor brain regions in 22q11.2 deletion carriers is predictive of autism-relevant traits.

DISCUSSION

In the present work, we describe a cross-species investigation of the neural determinants and developmental course of functional connectivity in 22q11DS, a highly penetrant genetic risk model for schizophrenia. We report converging cross-species evidence of developmental dysconnectivity in 22q11DS, with fMRI hyperconnectivity reverting to hypoconnectivity over puberty, both in LgDel mice and in people harboring a chromosomal 22q11.2 deletion. In the mouse, fMRI dysconnectivity is accompanied by GSK3β-dependent spine density alterations mirroring functional connectivity differences. In keeping with rodent findings, brain regions exhibiting developmental reconfiguration in human 22q11DS are enriched for synaptic-related genes that interact with GSK3β. Last, we report that functional dysconnectivity in somatomotor components of this network is predictive of social alterations in 22q11.2 deletion carriers. Collectively, our results provide evidence of synaptic-related developmental dysconnectivity in 22q11DS.

fMRI connectivity mapping has been previously used to describe network correlates of pathology in 22q11DS. Evidence of hypoconnectivity in hippocampal and key nodes of the DMN has been consistently reported in previous investigations of fMRI connectivity in individuals with 22q11DS (*23*, *54*, *55*). Initial studies investigating the developmental evolution of fMRI dysconnectivity in 22q11DS have also been reported, although with caveats related to the limited availability of fMRI investigations in children with 22q11DS. These investigations have shown that the developmental trajectory of fMRI connectivity within the DMN, in the HPC, and in the thalamocortical areas may be atypical in individuals with 22q11DS (*54*, *56*). Evidence of possible developmental alteration in functional connectome organization in 22q11DS has also been reported across development (*57*). Our study expands previous investigations in two main directions. First, by integrating human studies with controlled, parallel investigation in a rodent model, we were able to generate testable hypotheses regarding the developmental trajectory of fMRI dysconnectivity in 22q11DS with a degree of confidence currently unattainable in clinical research (*13*). Rodent investigations were instrumental in the identification of a critical developmental window during which cortical dysconnectivity markedly reconfigures in 22q11DS. Second, our cross-species work allowed probing the mechanisms underlying these findings. From a methodological standpoint, our results epitomize the potential of cross-species research in biologically decoding the mechanism of fMRI dysconnectivity in humans.

By longitudinally mapping fMRI connectivity in LgDel mice, we provide a detailed account of developmental dysconnectivity in an established rodent model of 22q11DS (*20*). The presence of reduced hippocampal connectivity in adult LgDel mice is in agreement with the results of fMRI studies in other rodent models of 22q11DS (*58*, *59*) and recapitulates functional neuroimaging findings that have been documented in individuals with 22q11DS (*23*, *54*). Extending these previous investigations, our work shows that this fMRI hypoconnectivity develops over puberty, is preceded by widespread cortical hyperconnectivity, and is plausibly mediated by synaptic-dependent mechanisms.

The presence of altered synaptic alterations is a feature shared by multiple transgenic mouse models of 22q11DS, where reduced synaptic density in hippocampal regions has been typically observed (*35*, *37*, *60*). We report that, in cortical and hippocampal regions, dendritic spine alterations are prominent and markedly evolve over puberty. The presence of supranumeral synapses and fMRI hyperconnectivity in cortical and hippocampal regions in prepubertal LgDel animals is broadly consistent with recent work linking synaptic surplus to aberrant fMRI coupling in a mouse model of syndromic autism (*10*). This finding is also consistent with our observation of aberrant extension of somatomotor connectivity networks in children with 22q11DS (Fig. 2C), where it could indicate altered synaptic refinement and impaired network maturation (*61*, *62*). Overall, the emerging model is one in which deficient synaptic pruning during early development is followed by compensatory (PFC) or overcompensatory (HPC) synaptic elimination over puberty. The biological mechanisms underlying aberrant synaptic elimination in hippocampal regions were not investigated here. However, the involvement of aberrant microglia-related signaling and synaptic elimination represents a possible explanation for this remodeling. In keeping with this notion, we recently found evidence of increased microglial complement systems C4 expression in adolescent LgDel mice, a phenotype that has been associated with aberrant synaptic pruning over puberty (*39*).

While the mechanisms leading to dendritic synaptic surplus in juvenile mice may be manifold, our pharmacological manipulations suggest that GSK3β inhibition is sufficient to prevent this phenotype in LgDel mice. Regional enrichment for GSK3β synaptic interactors in areas of human 22q11DS neural dysconnectivity corroborates the relevance of this finding for human 22q11.2 deletion carriers. Hyperactivity of GSK3β is etiologically linked to 22q11DS via Zdhhc8 haploinsufficiency, a hemizygously deleted genes in the 22q11.2 locus (*40*). From a mechanistic standpoint, these results are consistent with GSK3β's pivotal role in controlling synaptic development, function, and homeostasis (*41*). GSK3β hyperactivity may thus influence synaptic homeostasis via an indirect modulation of plasticity mechanisms underlying synapse formation and elimination (*63*) or by interfering with autophagic pathways essential for synapse maintenance (*10*, *64*). Recent evidence also points at a crucial role of microglia in mediating the phagocytosis of synaptic debris during pruning (*65*, *66*), a pathway in which GSK3β is also implicated (*67*). While our data plausibly link aberrant GSK3β signaling to juvenile fMRI hyperconnectivity, they do not conclusively establish whether fMRI hypoconnectivity is similarly GSK3β-dependent. The fact that this postpubertal phenotype was not rescued by developmental SB

administration may simply reflect a time-limited action of the drug or the involvement of GSK3β-independent synaptic elimination. In this respect, a contribution of microglial mechanisms or other known 22q11.2 synaptic interactors (i.e., COMT, DGCR8, RTN4R, and SEPT5) cannot be ruled out (fig. S13).

The observation of peri-pubertal dysconnectivity remodeling in LgDel mice and its confirmation in a large clinical cohort are of interest in the light of the high-risk 22q11DS that confers for both early and late onset neurodevelopmental disorders (*14*). While evidence of atypical developmental dysconnectivity has been reported in hippocampal (*54*) or thalamocortical areas (*25*), our results revealed widespread cortical hyperconnectivity in prepubertal 22q11DS individuals, a finding associated with aberrant extension of the somatomotor-network. The parallel identification of this phenotype in mice and human increases our confidence in this finding, despite the still limited number of fMRI scans available in prepubertal 22q11DS individuals. While the clinical relevance of this connectivity reconfiguration remains to be fully determined, our analyses revealed that dysconnectivity in sensory-motor areas was predictive of autism-related traits, specifically impairments in reciprocal social behavior. This notion is consistent with the observation of a disproportionately high enrichment of autism-relevant genes in the same regions undergoing developmental switching and with the developmental conceptualization of autism (and autism-related disorders) as dysconnectivity syndromes characterized by hyperconnectivity in childhood and hypoconnectivity in adult stages (*68*). It should also be noted that fMRI connectivity in somatomotor areas has been recently found to be associated with symptom severity in idiopathic autism (*69*). We, however, acknowledge that, albeit plausible and enticing, this association does not entail causality. Further proof of the specificity and replicability of this brain-behavior association will require extensions to larger patient cohorts and cross-referencing to other symptoms domains (e.g., psychosis-related traits), an analysis that was not feasible in the present study owing to the paucity of both brain and behavioral data in children with 22q11DS.

The reduced sociability that we observed in LgDel mice recapitulates social impairments described in individuals with 22q11DS (*70*, *71*). However, brain-behavior investigations in mice did not appear to directly align with corresponding human results. Specifically, as previously reported (*10*), we found that, in WT mice, connectivity within the DMN and its striatal components are positively correlated with social behavioral performance. However, this relationship was disrupted and, as such, uncorrelated with social behavior in LgDel mice. This finding is not entirely unexpected, owing to the evolutionary distance and the highly diverging substrate underlying higher-order socio-cognitive functions in rodents and humans. In rodents, social processing is strongly rooted in olfactory encoding, while, in humans, it involves processing of visual functions that are poorly developed in mice (*72*, *73*).

Of note, adult LgDel mice also exhibited cognitive dysfunction in the temporal-order memory domain, consistent with results in other mouse models of 22q11DS (*74*) and the observation of hippocampal-dependent memory alterations in humans (*75*). Developmental inhibition of GSK3β did not ameliorate social dysfunction at either age but was effective in reversing memory impairment in adult mice, as previously documented (*76*). The clear dissociation between early and late effect of GSK3β inhibition on connectivity and cognitive deficits suggests that fMRI connectivity reflects basic coupling mechanisms [e.g., dendritic spine integration; (*10*)] that are not necessarily directly related or relevant to higher-order cognitive functions related to brain plasticity, like temporal-order memory. As indicated by a growing body of evidence, synaptic plasticity can instead be profoundly impaired by GSK3β overactivity, resulting in aberrant long-term potentiation–like activity (*42*). GSK3β overactivity can also influence control of transcriptional and metabolic processes (*63*, *77*, *78*). Future investigations are required to disambiguate these contributions and relate them to specific symptoms and manifestations of 22q11DS.

A number of limitations in our work deserve to be mentioned. First, investigations of the developmental trajectory in 22q11DS individuals were not sufficiently powered to allow for a fine-grained description of the temporal evolution of fMRI dysconnectivity throughout adolescence and into young adulthood. Future studies are required to probe the precise trajectory of network dysconnectivity in 22q11DS across puberty. Second, our work employed cluster correction methods that are prone to producing false positives (*79*). However, the cross-species nature of our findings and their biological validation in a rodent model converge to support the validity of our results. Third, while medication use in 22q11DS individuals may have influenced our findings, the results from our mouse studies, which showed developmental dysconnectivity similar to that in 22q11DS individuals, suggest that this is unlikely to be the case. Future studies with larger clinical cohorts are needed to further investigate the potential influence of medications on these findings.

In conclusion, our work provides the first cross-species evidence of fMRI dysconnectivity in 22q11DS over puberty. Mouse and human studies converge to suggest that the observed fMRI alterations are underpinned by synaptic-dependent mechanisms, encompassing a pivotal involvement of GSK3β signaling. This developmental dysconnectivity is also predictive of social alterations in human 22q11.2 deletion carriers. Together, our results shed light on the etiopathological underpinnings of fMRI dysconnectivity in 22q11DS.

MATERIALS AND METHODS

Mouse studies

Ethical statement

Animal studies were conducted in accordance with the Italian Law (DL 26/2014, EU 63/2010, Ministero della Sanità, Roma) and the recommendations in the National Institutes of Health's *Guide for the Care and Use of Laboratory Animals*. Animal research protocols were reviewed and consented to by the animal care committee of the Istituto Italiano di Tecnologia and the Italian Ministry of Health specifically approved the study protocol (authorization no. 752/19 to A.G.).

Animals and experimental cohorts

Animals were housed under controlled temperature (21° ± 1°C) and humidity (60 ± 10%) and maintained on a 12-hour light/dark cycle, with food and water available ad libitum. LgDel mice [(Del(16Dgcr2-Hira)1Rak, the Jackson Laboratory) were backcrossed for more than 10 generations with C57BL/6J mice and genotyped as previously described (*27*). "Wild-type" (WT) littermates were used as control, WT mice.

Mouse fMRI and behavioral investigations encompassed a cross-sectional treatment protocol with four cohorts of age matched mice (mixed sexes): WT mice treated with SB [2 mg/kg, intraperitoneally (ip); WT SB, $n = 22$; $n = 12$ males and $n = 10$ females]; WT mice treated with VEH [dimethyl sulfoxide (DMSO; 2 mg/ml) in polyethylene glycol 400; WT, $n = 22$; $n = 14$ males and $n = 8$ females]; LgDel mice treated with SB [2 mg/kg, ip; (*76*); LgDel SB, $n = 23$; $n = 14$

males and $n = 9$ females); and LgDel mice treated with VEH (LgDel, $n = 21$; $n = 12$ males and $n = 9$ females). SB or VEH was administered every other day from PND7 to PND27 at 9:00 a.m. as previously described (*76*). The drug was initially dissolved in DMSO at a concentration of 20 mg/ml. On the days of injection, drug stock solutions were freshly diluted with polyethylene glycol 400 to achieve a final concentration of 2 mg/kg as in (*76*).

Mice underwent two sessions of fMRI: the first at the juvenile stage (PND35 ± 1) and the second after puberty (PND109 ± 3). Behavioral assessments of sociability were conducted on the same mice at the age of 30 ± 2 days, immediately before fMRI. Behavioral tasks in adulthood were conducted after the second imaging session. Before the second imaging session, two mice from the LgDel SB group exhibited health issues and were, therefore, removed from the study, resulting in a final sample size of $n = 23$. All behavioral testing and procedures were conducted during the light phase of the cycle. Experimenters were blind to mouse treatments during testing and behavioral scoring.

fMRI acquisition

For resting state fMRI, mice were anesthetized with isoflurane (5% induction), intubated, and artificially ventilated (2% maintenance) (*8*, *10*). After surgery, isoflurane was discontinued and replaced with halothane (0.8%). Functional data acquisition started 30 min after isoflurane cessation. Genotype-dependent variations in anesthesia sensitivity were assessed by recording minimal alveolar concentration of halothane as previously described (*10*, *38*). Two distinct cohorts of WT and LgDel mice at the juvenile and adult stages were included in this analysis (juvenile, PND35 to PND37: WT, $n = 8$; and LgDel, $n = 5$; and adult, PND150 ± 30: WT, $n = 11$; and LgDel, $n = 10$). No significant age × genotype interaction was detected (age × genotype interaction, $F = 0.77$, $P = 0.4$). These findings suggest that age × genotype interaction in anesthesia sensitivity did not significantly contribute as a confounding factor in our fMRI results. Ventilation parameters were adjusted to maintain normo-physiological p_aCO_2 (<40 mmHg) and p_aO_2 levels (>90 mmHg, corresponding to >98% hemoglobin saturation). fMRI images were acquired a 7-T MRI scanner (Bruker Biospin, Milan) with Bruker ParaVision software (v6) using a 72-mm birdcage transmit coil and a four-channel solenoid coil for signal reception (*29*). Single-shot BOLD fMRI time series were acquired using an echo-planar imaging (EPI) sequence with the following parameters: repetition time/echo time (TR/TE) of 1000/15 ms, flip angle of 60°, matrix of 98 × 98, field of view (FOV) of 2.3 cm by 2.3 cm, 18 coronal slices, and slice thickness of 550 μm for 1920 volumes.

fMRI connectivity analysis

fMRI images were preprocessed as previously described (*10*). Briefly, the initial 50 volumes of the time series were removed to allow for T1 and gradient thermal equilibration effects. Data were next despiked, motion corrected, skull stripped, and registered to a BOLD reference template. Motion traces of head realignment parameters (three rotations and three translations) and mean ventricular signal were used as nuisance covariates and regressed out. All fMRI time series were next band-pass filtered (0.01 to 0.1 Hz) and spatially smoothed with a full width at half maximum of 0.6 mm. Last, we carried out censoring of BOLD volumes flagged for high motion using a frame-wise displacement threshold greater that 0.05 mm.

To identify "hotspots" of dysconnectivity in a spatially unbiased fashion, we computed global functional connectivity at the voxel level. This metric quantifies the temporal correlation between fMRI signal of a voxel and that of all the other voxels in the brain. Global connectivity is predominantly skewed toward long-range connections, defined here as those exceeding 600 μm from a given voxel, which account for 99.77% of all brain voxels (*47*). Pearson's correlation scores were first transformed to z scores using Fisher's r-to-z transformation and then averaged to provide the final connectivity scores.

Global connectivity mapping identifies regions where connectivity is altered in relation to other brain areas. By examining the connectivity of these dysconnectivity foci, we could then determine which regions or networks show altered connectivity with the probed area. For this reason, we used global connectivity mapping as the primary measure of connectivity alterations in our study, and we systematically followed up global connectivity mapping with targeted seed-based network probing. Functional connectivity network mapping was carried out using a seed-based analysis by placing predefined seeds (3 × 3 × 1, voxels) in regions of interest selected based on our global connectivity results (fig. S1). Between-group differences were mapped using a two-tailed Student's t test ($|t| > 2$, $P < 0.05$) and FWER cluster corrected for multiple comparisons using a cluster defining threshold of $P < 0.05$ as implemented in FMRIB Software Library (FSL). Voxel-wise interaction between genotype and age factors was assessed using a linear mixed-effects model (lmer4 package in R) with within-subject variability as random intercept (+1|subject). The obtained t score maps were FWER cluster corrected using a cluster threshold of $P = 0.05$.

To depict effect size of mapped fMRI differences, z-scored fMRI connectivity from cubic volumes of interest (5 × 5 × 1) was extracted and plotted (fig. S1). All quantifications were plotted using raincloud plots (*80*). The resulting values were tested for statistical significance using a linear mixed-effects analysis. Brain regions showing connectivity differences in previous age × genotype interaction analysis (Fig. 1, E and F) were further investigated for the presence of sex × genotype interaction at both ages. These analyses did not provide evidence of any statistically significant sex × genotype interaction.

Dendritic spine quantification

To highlight dendritic spines of cortical and hippocampal pyramidal neurons for postmortem quantifications, 2 μl of AAV8–hSyn–green fluorescent protein (GFP; 10^{11} IU/ml) was bilaterally injected in lateral ventricles of newborn WT and LgDel mice at PND1. Four mice cohorts were analyzed at each developmental stage. Specifically, investigations in the PFC were carried out at the juvenile stage in $n = 4$ WT VEH mice ($n = 2$ males and $n = 2$ females), $n = 4$ WT SB ($n = 3$ males and $n = 1$ female), $n = 6$ LgDel VEH ($n = 1$ male and $n = 5$ females), $n = 7$ LgDel SB ($n = 4$ males and $n = 3$ females); PFC investigation in adult mice were conducted in $n = 4$ WT VEH mice ($n = 3$ males and $n = 1$ female), $n = 4$ WT SB ($n = 2$ males and $n = 2$ females), $n = 4$ LgDel VEH ($n = 2$ males and $n = 2$ females), and $n = 4$ LgDel SB ($n = 2$ males and $n = 2$ females). Spine counting in HPC was conducted in a subset of the same animals. Specifically, at the juvenile stage, we used $n = 4$ WT VEH mice ($n = 2$ males and $n = 2$ females), $n = 4$ WT SB ($n = 3$ males and $n = 1$ female), $n = 4$ LgDel VEH ($n = 1$ male and $n = 3$ females), and $n = 4$ LgDel SB ($n = 2$ males and $n = 2$ females) mice; for HPC counts in adult mice, we used $n = 4$ WT VEH ($n = 2$ males and $n = 2$ females), $n = 4$ WT SB ($n = 2$ males and $n = 2$ females), $n = 4$ LgDel VEH ($n = 2$ males and $n = 2$ females), and $n = 4$ LgDel SB ($n = 2$ males and $n = 2$ females). VEH or SB administration was carried out from PND7 to PND27 as described above. At PND33

(juvenile) or PND112 (adult), mice were euthanized via transcardial 4% paraformaldehyde–phosphate-buffered saline perfusion. Brains were sectioned with a vibratome (Leica) at 50 μm (coronal) and processed for free-floating immunofluorescence. Briefly, tissue was incubated in blocking solution (5% horse serum in 0.5% PBTriton) 1 hour at room temperature and subsequently incubated overnight at 4°C in primary antibody solution using Rabbit anti-GFP (1:1000; Thermo Fisher Scientific, A6455). The following day, sections were rinsed three times in 0.5% PBTriton and incubated overnight at 4°C in secondary antibody solution using goat anti-rabbit Oregon Green 488 (1:500; Invitrogen, 011038). Next, samples were rinsed in PBTriton, counterstained with 4′,6-diamidino-2-phenylindole (1:1000), and mounted with AquaPolymount (Polysciences). High-resolution images dendritic spines were acquired using a Nikon A1 Eclipse confocal microscope equipped with NIS-Elements AR v4.20.03 software (Nikon) and a 60× plan-apo oil immersion objective with a ×2 digital magnification [1024 × 1024 pixels (px), 0.1 μm/px]. Spine density quantification was performed on basal dendrites of layer V PFC pyramidal neurons (bregma from 2.58 to 2.34 mm) and on apical dendrites of CA1 hippocampal neurons (bregma from −2.92 to −3.40). Spine counting was performed using the Filament function of Imaris Microscopy Image Analysis Software by Bitplane (v7.2.3). A single first-order dendrite per neuron was analyzed for a total of 10 to 15 neurons for each animal. The analysis was performed by an operator blind to the genotype. Data are expressed as spine number per micrometer of dendrite length. Statistical analysis was performed using Prism GraphPad (v9.2).

Behavioral testing

Habituation/dishabituation social interaction test

Juvenile mice were tested as previously reported (*81*) in lightly illuminated (5 ± 1 lux) GR900 Tecniplast cages (904 cm^2). Mice were placed individually in the testing cage 1 hour before the test. A stimulus mouse of the same sex, strain, and age was introduced into the testing cage for a 1-min interaction. After the 1-min trial, the stimulus mouse was removed for 3 min and placed back in its home cage. This procedure was repeated four times. Subsequently, a fifth 1-min dishabituation trial was conducted, introducing a new stimulus mouse to the testing cage. The time spent interacting (interaction time), which included the sum of nose-to-nose sniffing, anogenital sniffing, and following, was recorded across all trials. The interaction time across the first four trials was summed up and analyzed using a two-way ANOVA.

SCPP test

Juvenile mice also underwent a SCPP test, adapted from a previous study (*82*). The test was conducted in a three-chamber arena, with each chamber measuring 20 cm by 40 cm by 22 cm. Two different environments were used for the conditioning sessions, with each environment represented by different types of bedding: corncob bedding (SCOBIS DUE G8, Mucedola) and aspen bedding (SCOBIS QUATTRO, Mucedola). To prevent any bias toward one environment from affecting the results, a 30-min preconditioning test was conducted on the first day. In this test, both environments were randomly allocated to each of the two external chambers. To mitigate potential natural biases that might obscure the effects of social conditioning, the less preferred context was paired with social enrichment. Mice that displayed a preconditioning preference of more than 70% for one environment type were excluded from subsequent conditioning. This led to the exclusion of one WT mouse, two LgDel mice, and three LgDel SB mice, resulting in a final sample size of WT, $n = 22$; LgDel, $n = 21$; WT SB, $n = 22$; and LgDel SB, $n = 22$.

After the preconditioning phase, mice underwent a 24-hour social conditioning session with their cagemates in the environment where they initially spent less time. Twenty-four hours later, they were placed in the other environment type without their cagemates. The next day, a 30-min post-conditioning session was conducted following the same procedure as the preconditioning session. The performance in the preconditioning and post-conditioning sessions within the same group was assessed through a paired Student's *t* test. To address potential variations in locomotory behavior within the apparatus and baseline preferences, comparisons between experimental conditions were made using a preference score. This score was calculated as the percentage of time spent in the social context, normalized by the total time in compartments, with baseline values subtracted as described in (*83*). Data were analyzed using a two-way ANOVA with genotype and treatment factors followed by a Sidak's multiple comparisons test.

Three-chambered social approach tasks

After the second imaging session, adult mice were tested in a three chamber test, following the protocol described in (*84*). The apparatus consisted of a three-chamber box, with each chamber measuring 20 cm by 40 cm by 22 cm, featuring two sliding doors (5 cm by 8 cm) that opened into the central compartment and two wire cages (15 cm in height) where a "stimulus" mouse was introduced. The stimulus mouse was an experimentally naïve mouse, with no prior interactions with the testing mouse. These stimulus mice were of the same sex, background, aged between 2 and 6 months, and approximately matched in body weight to the testing mouse (within 5 g). Before the task, the stimulus mice were habituated to the wire cups 4 days in advance to minimize signs of agitation and aggression.

The task commenced with a 10-min habituation phase in the central compartment, followed by an additional 10-min habituation phase encompassing all three chambers. The "sociability phase" (10 min) began immediately after the habituation phase. During this phase, the testing mouse was introduced into the central zone and allowed to explore side compartments, one containing an empty cup and the other containing a cup with a novel stimulus mouse. The locations of the empty and "mouse" cups were randomly assigned. A "sociability index" was calculated as the difference between the time spent sniffing the mouse cup and the time spent sniffing the empty cup, normalized by the total time spent sniffing. Subsequently, a "social novelty phase" (10 min) was conducted, with a new stimulus mouse introduced in the empty cup. A "social novelty index" was calculated as the difference between the time spent sniffing the cup with the new stimulus mouse and the cup with the old stimulus mouse, normalized by the total time spent sniffing.

One hour later, a "social memory phase" (10 min) was carried out. A "social memory sniffing index" was calculated as the difference between the time spent sniffing the cup with the newest stimulus mouse and the cup hosting the stimulus mouse from the sociability phase, normalized by the total time spent sniffing. In this phase, the same stimulus mouse from the sociability phase was placed in the same side as before, while a novel stimulus mouse was placed in the other side. Two LgDel animals were exempted from testing because of health issues (corneal opacity), resulting on a final sample of WT, $n = 21$; LgDel, $n = 20$; WT SB, $n = 22$; and LgDel SB, $n = 22$. Data were analyzed using a two-way ANOVA with genotype and treatment factors followed by a Sidak's multiple comparisons test.

Temporal-order memory task

Adult mice also underwent a temporal-order memory task (*85*). This task assesses recency discrimination by measuring the time spent exploring two objects encountered at different time points. An intact temporal-order memory is indicated by more time spent exploring the object encountered earlier compared to the newer one. The test was conducted in an arena measuring 43 cm by 43 cm. The animals were habituated in the same arena the day before for a duration of 1 hour. The task consisted of three sessions, each lasting 5 min, with 1-hour intervals between the first two sessions and a 3-hour interval between the second and the third sessions, as described in (*85*).

In the first and second sessions, two different couples of identical objects were introduced into the arena, and the animals were free to explore them. In the last session, one copy of the object from the first phase and one copy of the object from the second phase were placed in the arena. The position of objects in this phase was randomly selected and counterbalanced across the different groups. A discrimination index was computed as the disparity between the time spent exploring the object from the first phase and the object from the second phase, divided by the total time spent exploring both objects. A discrimination index exceeding 0 suggests intact temporal-order memory. Mice who did not complete at least 2 s of exploration during the experimental phases were excluded from the analysis. One animal was excluded for this reason. Another animal was exempted from testing because of health issues (corneal opacity). Data were analyzed using a two-way ANOVA with genotype and treatment factors followed by a Sidak's multiple comparisons test.

Partial least square analysis

Partial least squares correlation (PLSC) analysis (*44*) was used to assess the relationship between resting-state functional connectivity and behavior in our mice cohort. PLSC is a multivariate method that finds brain-behavioral latent components (LCs) that maximally covary while being uncorrelated to other LVs. The null hypothesis that the observed brain-behavior relationship could be due to chance was tested via permutation testing (1000 iterations) of the behavioral data. To prevent LCs from being driven by intergroup differences, permutation was performed within groups (*86*). The stability of the contribution of each brain and behavioral element was assessed via bootstrapping with replacement (1000 iterations) and also computed within experimental group to avoid covariance patterns being driven by group differences (*86*). PLSC was carried out between the behavior at each age and connectivity in default mode and ventral hippocampal network. These networks encompass brain regions implicated in the behaviors assessed (*10*, *46*, *47*). Treatment was entered as a binary design variable in the behavioral matrix to assess the genotype-specific contribution of treatment to the observed brain-behavioral covariance.

Human studies

Participants

The human sample used in this study comprised 256 participants, recruited from three research sites. The sample was divided into two cross-sectional cohorts: The first cohort consisted of individuals aged 6 to 11 years old, including 21 molecularly confirmed 22q11.2 deletion carriers (22q11DS) and 31 demographically comparable HCs. The second cohort encompassed participants aged from puberty to 30 years (referred to hereafter as postpuberty), comprising HCs ($n = 86$) and 22q11DS ($n = 118$). As we lacked direct measures of pubertal onset, 11 years of age was chosen as a cutoff between the childhood and postpuberty groups across sexes on the basis of epidemiological studies estimating 10 to 11 as crucial ages for puberty onset (*87*). Deletion carriers and HCs were matched on the basis of age and sex. Aggregate and site-specific demographics are reported in Table 1 and table S1, respectively.

Participants with neurological or medical conditions unrelated to 22q11.2 deletion, insufficient fluency in English, substance or alcohol abuse and/or dependence within the past 6 months, as well as HC individuals meeting diagnostic criteria for any major mental disorders (e.g., psychotic disorders, bipolar disorder, and autism) upon administration of the Structured Clinical Interview for DSM-IV/V Axis I Disorder were excluded from the study. HC individuals diagnosed with ADHD ($n = 1$ child and $n = 3$ postpubertal individuals) and/or a history of anxiety or depressive episodes ($n = 1$ child and $n = 10$ postpubertal individuals) were included in our sample because of the high prevalence of these conditions (*25*, *88*, *89*). Of the $n = 16$ HC individuals with a diagnosis of anxiety, mood disorders, or ADHD, $n = 5$ did also report use of medication, and one individual was taking anxiolytic medications in absence of diagnosed psychiatric conditions (Table 1). All these individuals were included in our analyses.

To control for a possible confounding contribution of HC individuals with a mental health diagnosis or receiving medication, we also repeated age × genotype interaction global connectivity mapping excluding these 16 participants ($n = 2$ children and $n = 14$ postpuberty individuals).

Adult participants provided written consent, while participants under the age of 18 years required written consent from their parents or guardians. All procedures and informed consent documents received approval from the Institutional Review Board at each academic center.

Clinical assessment

Autism-related traits in participants were assessed using the Social Responsiveness Scale (SRS) for children (6 to 17 years old) or adults (18 years and older) (*90*), in addition to an Autistic Diagnostic Interview. Total SRS *T* score was used in further analyses (detailed below) as a measure of reciprocal social behavior. Verbal intelligence quotient (IQ) and nonverbal IQ were evaluated using the Wechsler Abbreviated Scale of Intelligence–2 (WASI-2), which included the WASI-2 Vocabulary and WASI Matrix Reasoning tests. The scores from these tests were combined to derive a WASI full-scale IQ (*91*), as detailed in Table 1. For the assessment of neuropsychiatric diagnoses and symptomatology, participants were administered the Structured Clinical Interview for DSM-IV Axis I Disorders, with an additional developmental disorders module (*92*), the Structured Interview for Psychosis-Risk Syndromes (*93*), the Autistic Diagnostic Observation Schedule (*94*), and the Brief Psychiatric Rating Scale [see (*95*) for recruitment and clinical assessment details].

fMRI acquisition

fMRI time series were obtained from three different sites: UCLA, SUNY, and KCL. At UCLA, the images were acquired using two different scanners. One subset of individuals from the UCLA sample (childhood: HC, $n = 21$; and 22q11DS, $n = 11$; postpuberty: HC, $n = 24$; and 22q11DS, $n = 32$) was scanned on a 3-T Siemens Tim Trio Scanner equipped with a 12-channel head coil receiver. The acquisition parameters for these resting state fMRI BOLD images were as follows: voxel size of 3.0 mm by 3.0 mm by 4.0 mm, TE of 30 ms, TR of 2000 ms, flip angle of 90°, matrix size of 64 × 64, FOV of 192,

34 axial slices, and a slice thickness of 4.0 mm for 152 volumes. The other subset from UCLA (childhood: HC, $n = 5$; and 22q11DS, n = 7; postpuberty: HC, $n = 7$; and 22q11DS, $n = 21$) was imaged on a 3-T Siemens Magnetom Prisma Fit scanner equipped with a 32-channel head coil receiver. The acquisition parameters for this subset were voxel size of 2.0 mm by 2.0 mm by 2.0 mm, TE of 37 ms, TR of 800 ms, flip angle of 52°, matrix size of 104 × 104, FOV = 208, 72 axial slices, and a slice thickness of 2.0 mm for 420 volumes. Individuals from the SUNY sample (postpuberty: HC, $n = 28$; and 22q11DS, $n = 44$) were imaged on a 3-T Siemens Tim Trio Syngo MR B17 scanner with an eight-channel head coil receiver. The acquisition parameters for fMRI BOLD images at SUNY were voxel size of 4.0 mm by 4.0 mm by 4.0 mm, TE of 30 ms, TR of 2000 ms, flip angle of 90°, matrix size of 64 × 64, FOV of 256, 34 axial slices, and a slice thickness of 4.0 mm for 152 volumes. At KCL (childhood: HC, $n = 5$; and 22q11DS, $n = 3$; postpuberty: HC, $n = 27$; and 22q11 DS, $n = 21$), the images were acquired using a 3-T GE Signa HDx scanner, with the following acquisition parameters: voxel size of 4.0 mm by 4.0 mm by 4.0 mm, TE of 30 ms, TR of 2000 ms, flip angle of 90°, matrix size of 64 × 64, FOV of 256, 34 axial slices, and a slice thickness of 4.0 mm for 152 volumes. Across all sites, participants were instructed to keep their eyes open during the acquisition.

fMRI preprocessing

Images were preprocessed using the preconfigured "preprocessing" pipeline (available at https://doi.org/10.5281/zenodo.14761241 and at https://github.com/FCP-INDI/C-PAC/blob/master/CPAC/resources/configs/pipeline_config_preproc.yml) of the Configurable Pipeline for the Analysis of Connectomes (https://fcp-indi.github.io/) (*96*). Briefly, functional scans were slice-timing corrected and motion corrected using rigid-body, six-parameter transformations. Nuisance variable regression was then performed on the motion corrected data including the regression of a 24-parameter model of motion (including the six motion parameters, their square, their derivatives, and the square of their derivatives), five noise signals identified using CompCor obtain from White Matter, and the mean cerebrospinal fluid signal. Scans were then filtered using a band-pass filter only retaining frequencies between 0.01 and 0.1 Hz and normalized to MNI 152 template with linear and nonlinear registration. Smoothing was performed using a Gaussian kernel of 6-mm full width at half maximum. fMRI volumes in which the sum of mean frame-wise displacement across the six rigid-body parameters exceeded 0.5 mm were scrubbed. Participants with more than 40% of frames scrubbed were excluded from further analyses.

fMRI connectivity analyses

The objective of these analyses was to assess whether the functional dysconnectivity signature observed in the mouse model is translationally conserved in the human cohort. We conducted the same functional analyses in the human dataset for both age groups to maximize cross-species comparability. Specifically, we used global connectivity mapping to create an unbiased mapping of functional connectivity differences within a 25% gray-matter probability mask. To minimize the impact of interscanner variability on our results, we harmonized our global connectivity maps using Combat, a state-of-the-art tool based on an empirical Bayes formulation that minimizes between-site variability (*97*). Between-group differences between 22q11DS and HC were then analyzed while controlling for the effects of sex and number of retained volumes and were FWER cluster corrected for multiple comparisons as implemented in FSL ($|t| > 2.0$, $P < 0.05$), for each of the two age groups separately. Two-way ANOVA was then used to test the interaction between age group (childhood and postpuberty) and genotype (HC and 22q11DS). Similarly to the mouse model, we used seeds placed in foci of altered global functional connectivity, as illustrated in fig. S5, to compute seed-based functional connectivity.

We limited these investigations to seeds broadly confined within well-characterized anatomical regions (i.e., the opercular cortex and postcentral gyrus), which makes them suitable for subsequent network-level mapping. A third large cluster of dysconnectivity also survived cluster correction in the age × genotype interaction map (Fig. 2B, left hemisphere). Because of the large and anatomically nonspecific extension of this cluster, we did not include it in further seed-based mapping, as its use would produce functional connectivity maps devoid of any network specificity. We thus did not further investigate the functional contribution of this cluster in any subsequent analysis. We additionally investigated fMRI connectivity maps obtained using the HPC and the PFC as seeds, because these two regions exhibited robust functional dysconnectivity in our mouse studies. We then calculated between-group differences and the age × genotype interaction of these seed-based maps using the same method used for global functional connectivity. Nonlinear developmental trajectories of global connectivity in areas undergoing significant reconfiguration were characterized using GAMMs (*34*). A GAMM was fit to predict global connectivity from the smoothed effect of age and genotype for each area of interest (opercular cortex, postcentral gyrus, and HPC), resulting in separate smooths for each group, 22q11DS and HC. Age ranges in which global connectivity between the two genotypes significantly differed were defined as age ranges where the 95% confidence interval of the genotype difference in age smooths did not include zero.

For the subset of 22q11 deletion carriers with available Social Responsiveness Scale (SRS) scores (childhood, $N = 18$; and postpuberty, $N = 111$), the relationship between 22q11DS-related functional dysconnectivity and autism-related behaviors was assessed using a voxel-wise linear model. The model used functional connectivity as a predictor of total SRS T score and examined its interaction with age group while controlling for the effects of sex and retained volumes. By including the interaction between functional connectivity and age group in the model, we were able to identify areas where the relationship between connectivity and SRS followed an age-specific pattern. This model was applied to three different voxel-wise connectivity maps: (i) global connectivity, (ii) seed-based maps of the postcentral gyrus, and (iii) seed-based maps of the opercular cortex. Each resulting age × fMRI connectivity interaction map was FWER cluster corrected for multiple comparisons ($|t| > 2.0$, $P < 0.05$). In Fig. 5B, we report a post hoc visualization of the interaction direction and the distribution of individual points, using a scatterplot to depict subject-wise SRS scores and corresponding mean operculum-to-postcentral gyrus fMRI connectivity. This plot is for visualization purposes and should not be considered an independent test.

Gene expression decoding and enrichment analysis

To probe which molecular mechanism might be involved in functional dysconnectivity of 22q11DS patients, we carried out a gene decoding and enrichment analysis. Gene expression decoding, as implemented by NeuroVault (*98*), aims at identifying genes whose spatial expression in the brain is similar to spatial patterns of functional connectivity. Briefly, a linear model is used to estimate spatial similarity between pattern of functional connectivity maps and individual gene expression maps for each of the 20,787 genes of the Allen Institute Human Brain Gene Expression atlas in each of the six donor's brain. Gene and donor-specific slopes are then assessed

using a one-sample *t* tests. The results of this *t* test are then multiple comparisons corrected, and only the genes surviving false discovery rate (FDR) at $q < 0.05$ are used in the following analyses. In the current study, areas undergoing hyperconnectivity-to-hypoconnectivity reconfiguration over development (i.e., 22q11-related dysconnectivity) are represented by positive *t* values in our voxel-wise global connectivity age × genotype interaction *t* maps. Hence, we restricted our search to genes that were positively correlated with our age × genotype interaction map (i.e., genes that were more expressed in areas of functional dysconnectivity). This resulted in a gene list of $N = 3897$ decoded genes, whose spatial expression positively correlates with areas of hyperconnectivity-to-hypoconnectivity reconfiguration in 22q11DS.

First, to test the hypothesis that synaptic mechanisms could be implicated in the observed dysconnectivity in human 22q11DS too, we performed gene enrichment analyses between the decoded genes and GO terms, identifying genes implicated in synaptic signaling, as reported by (*49*). Furthermore, we also tested the hypothesis of a significant enrichment between decoded genes and GO terms related to glial-related synaptic remodeling, given their involvement in this process (*39*).

Next, we set out to fully ascertain the parallelism between the dysconnectivity we observed in LgDel mice and 22q11 deletion carriers, specifically by looking at whether the decoded genes would be enriched for GSK3β-related synaptic genes. To do this, we obtained a broad list of GSK3β-interacting genes using protein-protein interaction analysis in the STRING database (*99*), with a medium confidence setting (0.4) and allowing up to 500 interactors. Given the broadness of this initial list and mouse-derived evidence of a mechanistic involvement of synaptic processes in functional dysconnectivity, we then increased its specificity by pruning the initial GSK3β interactors to only include genes involved in synaptic processes, as per our hypothesis guided by dendritic spine investigations. Specifically, we used the Syngo (*50*) synaptic gene list (which includes genes involved in biological processes in the presynapse and in the post-synapse, synaptic metabolism, synaptic signaling, transport, and synaptic organization) to reduce the initial $n = 501$ GSK3β interactors to $n = 113$ GSK3β-synaptic interactors. Full gene lists for GO terms and GSK3β interactomes are reported in table S4. Last, we exploited gene enrichment analyses to assess the clinical relevance of the functional dysconnectivity signature that we observed. Specifically, we performed gene enrichment analyses between the decoded genes and previously published disorder-relevant gene lists [(*51*, *52*, *100*, *101*) and https://gene.sfari.org, downloaded in April 2023]. A generative null model was used to assess the specificity of the observed enrichment for the spatial topography of our developmental dysconnectivity pattern. To this aim, we used a spatial autocorrelation preserving generative null model (*102*) to generate $k = 1000$ surrogate maps whose spatial autocorrelation matched that of the empirical developmental dysconnectivity (i.e., global connectivity age × genotype interaction) map. We then applied gene decoding to each surrogate map and performed gene enrichment analysis between the resulting decoded genes and any other gene lists of interest to us (i.e., the GO terms, the synaptic interactors of GSK3B, and the disorder-relevant gene lists), yielding 1000 overlap sizes for each of these lists of interests. We then compared the OR of the enrichment resulting from our empirical developmental dysconnectivity map with the 95th percentile of generated null distribution of OR.

Before all enrichment analyses, all gene lists were pruned to only include protein coding genes expressed in the brain [$N = 16796$ genes; (*51*)], which was, hence, considered as the background pool. For all gene enrichment analyses, OR and hypergeometric *P* values for enrichment analyses were computed using code publicly available at https://doi.org/10.5281/zenodo.13991845 and https://github.com/mvlombardo/utils/blob/master/genelistOverlap.R. FDR correction was applied to correct for multiple comparisons where appropriate, and corrected *q* values are reported for all enrichments.

Supplementary Materials

The PDF file includes:

Figs. S1 to S13
Table S1
Legends for tables S2 to S4

Other Supplementary Material for this manuscript includes the following:

Tables S2 to S4

REFERENCES AND NOTES

1. R. A. Vasa, S. H. Mostofsky, J. B. Ewen, The disrupted connectivity hypothesis of autism spectrum disorders: Time for the next phase in research. *Biol. Psychiatry Cogn. Neurosci. Neuroimaging* **1**, 245–252 (2016).
2. A. Harikumar, K. P. Solovyeva, M. Misiura, A. Iraji, S. M. Plis, G. D. Pearlson, J. A. Turner, V. D. Calhoun, Revisiting functional dysconnectivity: A review of three model frameworks in schizophrenia. *Curr. Neurol. Neurosci. Rep.* **23**, 937–946 (2023).
3. E. T. Bullmore, A. Fornito, Making connections: Biological mechanisms of human brain (Dys) connectivity. *Biol. Psychiatry* **93**, 384–385 (2023).
4. M. P. van den Heuvel, O. Sporns, A cross-disorder connectome landscape of brain dysconnectivity. *Nat. Rev. Neurosci.* **20**, 435–446 (2019).
5. V. Zerbi, M. Pagani, M. Markicevic, M. Matteoli, D. Pozzi, M. Fagiolini, Y. Bozzi, A. Galbusera, M. L. Scattoni, G. Provenzano, A. Banerjee, F. Helmchen, M. A. Basson, J. Ellegood, J. P. Lerch, M. Rudin, A. Gozzi, N. Wenderoth, Correection: Brain mapping across 16 autism mouse models reveals a spectrum of functional connectivity subtypes. *Mol. Psychiatry* **27**, 3920–3921 (2022).
6. D. H. Geschwind, P. Levitt, Autism spectrum disorders: Developmental disconnection syndromes. *Curr. Opin. Neurobiol.* **17**, 103–111 (2007).
7. K. J. Friston, C. D. Frith, Schizophrenia: A disconnection syndrome. *Clin. Neurosci.* **3**, 89–97 (1995).
8. A. Bertero, A. Liska, M. Pagani, R. Parolisi, M. E. Masferrer, M. Gritti, M. Pedrazzoli, A. Galbusera, A. Sarica, A. Cerasa, M. Buffelli, R. Tonini, A. Buffo, C. Gross, M. Pasqualetti, A. Gozzi, Autism-associated 16p11.2 microdeletion impairs prefrontal functional connectivity in mouse and human. *Brain* **141**, 2055–2065 (2018).
9. L. E. Suarez, R. D. Markello, R. F. Betzel, B. Misic, Linking structure and function in macroscale brain networks. *Trends Cogn. Sci.* **24**, 302–315 (2020).
10. M. Pagani, N. Barsotti, A. Bertero, S. Trakoshis, L. Ulysse, A. Locarno, I. Miseviciute, A. De Felice, C. Canella, K. Supekar, A. Galbusera, V. Menon, R. Tonini, G. Deco, M. V. Lombardo, M. Pasqualetti, A. Gozzi, mTOR-related synaptic pathology causes autism spectrum disorder-associated functional hyperconnectivity. *Nat. Commun.* **12**, 6084 (2021).
11. F. Rocchi, C. Canella, S. Noei, D. Gutierrez-Barragan, L. Coletta, A. Galbusera, A. Stuefer, S. Vassanelli, M. Pasqualetti, G. Iurilli, S. Panzeri, A. Gozzi, Increased fMRI connectivity upon chemogenetic inhibition of the mouse prefrontal cortex. *Nat. Commun.* **13**, 1056 (2022).
12. S.-J. Hong, J. T. Vogelstein, A. Gozzi, B. C. Bernhardt, B. T. T. Yeo, M. P. Milham, A. Di Martino, Toward neurosubtypes in autism. *Biol. Psychiatry* **88**, 111–128 (2020).
13. A. Gozzi, V. Zerbi, Modeling brain dysconnectivity in rodents. *Biol. Psychiatry* **93**, 419–429 (2023).
14. R. Gur, A. Bassett, D. McDonald-McGinn, C. Bearden, E. Chow, B. Emanuel, M. Owen, A. Swillen, M. Van den Bree, J. Vermeesch, A neurogenetic model for the study of schizophrenia spectrum disorders: The International 22q11.2 Deletion Syndrome Brain Behavior Consortium. *Mol. Psychiatry* **22**, 1664–1672 (2017).
15. C. R. Marshall, D. P. Howrigan, D. Merico, B. Thiruvahindrapuram, W. Wu, D. S. Greer, D. Antaki, A. Shetty, P. A. Holmans, D. Pinto, M. Gujral, W. M. Brandler, D. Malhotra, Z. Wang, K. V. F. Fajarado, M. S. Maile, S. Ripke, I. Agartz, M. Albus, M. Alexander, F. Amin, J. Atkins, S. A. Bacanu, R. A. Belliveau Jr, S. E. Bergen, M. Bertalan, E. Bevilacqua, T. B. Bigdeli, D. W. Black, R. Bruggeman, N. G. Buccola, R. L. Buckner, B. Bulik-Sullivan, W. Byerley, W. Cahn, G. Cai, M. J. Cairns, D. Campion, R. M. Cantor, V. J. Carr, N. Carrera,

S. V. Catts, K. D. Chambert, W. Cheng, C. R. Cloninger, D. Cohen, P. Cormican, N. Craddock, B. Crespo-Facorro, J. J. Crowley, D. Curtis, M. Davidson, K. L. Davis, F. Degenhardt, J. D. Favero, L. E. De Lisi, D. Dikeos, T. Dinan, S. Djurovic, G. Donohoe, E. Drapeau, J. Duan, F. Dudbridge, P. Eichhammer, J. Eriksson, V. Escott-Price, L. Essioux, A. H. Fanous, K.-H. Farh, M. S. Farrell, J. Frank, L. Franke, R. Freedman, N. B. Freimer, J. I. Friedman, A. J. Forstner, M. Fromer, G. Genovese, L. Georgieva, E. S. Gershon, I. Giegling, P. Giusti-Rodríguez, S. Godard, J. I. Goldstein, J. Gratten, L. de Haan, M. L. Hamshere, M. Hansen, T. Hansen, V. Haroutunian, A. M. Hartmann, F. A. Henskens, S. Herms, J. N. Hirschhorn, P. Hoffmann, A. Hofman, H. Huang, M. Ikeda, I. Joa, A. K. Kähler, R. S. Kahn, L. Kalaydjieva, J. Karjalainen, D. Kavanagh, M. C. Keller, B. J. Kelly, J. L. Kennedy, Y. Kim, J. A. Knowles, B. Konte, C. Laurent, P. Lee, S. H. Lee, S. E. Legge, B. Lerer, D. L. Levy, K.-Y. Liang, J. Lieberman, J. Lönnqvist, C. M. Loughland, P. K. E. Magnusson, B. S. Maher, W. Maier, J. Mallet, M. Mattheisen, M. Mattingsdal, R. W. McCarley, C. M. Donald, A. M. McIntosh, S. Meier, C. J. Meijer, I. Melle, R. I. Mesholam-Gately, A. Metspalu, P. T. Michie, L. Milani, V. Milanova, Y. Mokrab, D. W. Morris, B. Müller-Myhsok, K. C. Murphy, R. M. Murray, I. Myin-Germeys, I. Nenadic, D. A. Nertney, G. Nestadt, K. K. Nicodemus, L. Nisenbaum, A. Nordin, E. O'Callaghan, C. O'Dushlaine, S.-Y. Oh, A. Olincy, L. Olsen, F. A. O'Neill, J. Van Os, C. Pantelis, G. N. Papadimitriou, E. Parkhomenko, M. T. Pato, T. Paunio, Psychosis Endophenotypes International Consortium, D. O. Perkins, T. H. Pers, O. Pietiläinen, J. Pimm, A. J. Pocklington, J. Powell, A. Price, A. E. Pulver, S. M. Purcell, D. Quested, H. B. Rasmussen, A. Reichenberg, M. A. Reimers, A. L. Richards, J. L. Roffman, P. Roussos, D. M. Ruderfer, V. Salomaa, A. R. Sanders, A. Savitz, U. Schall, T. G. Schulze, S. G. Schwab, E. M. Scolnick, R. J. Scott, L. J. Seidman, J. Shi, J. M. Silverman, J. W. Smoller, E. Söderman, C. C. A. Spencer, E. A. Stahl, E. Strengman, J. Strohmaier, T. S. Stroup, J. Suvisaari, D. M. Svrakic, J. P. Szatkiewicz, S. Thirumalai, P. A. Tooney, J. Veijola, P. M. Visscher, J. Waddington, D. Walsh, B. T. Webb, M. Weiser, D. B. Wildenauer, N. M. Williams, S. Williams, S.H. Witt, A. R. Wolen, B. K. Wormley, N. R. Wray, J. Q. Wu, C. C. Zai, R. Adolfsson, O. A. Andreassen, D. H. R. Blackwood, E. Bramon, J. D. Buxbaum, S. Cichon, D. A. Collier, A. Corvin, M. J. Daly, A. Darvasi, E. Domenici, T. Esko, P. V. Gejman, M. Gill, H. Gurling, C. M. Hultman, N. Iwata, A. V. Jablensky, E. G. Jönsson, K. S. Kendler, G. Kirov, J. Knight, D. F. Levinson, Q. S. Li, S. A. McCarroll, A. M. Quillin, J. L. Moran, B. J. Mowry, M. M. Nöthen, R. A. Ophoff, M. J. Owen, A. Palotie, C. N. Pato, T. L. Petryshen, D. Posthuma, M. Rietschel, B. P. Riley, D. Rujescu, P. Sklar, D. S. Clair, J. T. R. Walters, T. Werge, P. F. Sullivan, M. C. O'Donovan, S. W. Scherer, B. M. Neale, J. Sebat, CNV and Schizophrenia Working Groups of the Psychiatric Genomics Consortium, Contribution of copy number variants to schizophrenia from a genome-wide study of 41,321 subjects. *Nat. Genet.* **49**, 27–35 (2017).

16. S. Oskarsdottir, M. Vujic, A. Fasth, Incidence and prevalence of the 22q11 deletion syndrome: A population-based study in Western Sweden. *Arch. Dis. Child.* **89**, 148–151 (2004).
17. D. M. McDonald-McGinn, K. E. Sullivan, B. Marino, N. Philip, A. Swillen, J. A. Vorstman, E. H. Zackai, B. S. Emanuel, J. R. Vermeesch, B. E. Morrow, P. J. Scambler, A. S. Bassett, 22q11.2 Deletion syndrome. *Nat. Rev. Dis. Primers.* **1**, 15071 (2015).
18. M. Schneider, M. Debbane, A. S. Bassett, E. W. Chow, W. L. Fung, M. van den Bree, M. Owen, K. C. Murphy, M. Niarchou, W. R. Kates, K. M. Antshel, W. Fremont, D. M. McDonald-McGinn, R. E. Gur, E. H. Zackai, J. Vorstman, S. N. Duijff, P. W. Klaassen, A. Swillen, D. Gothelf, T. Green, A. Weizman, T. Van Amelsvoort, L. Evers, E. Boot, V. Shashi, S. R. Hooper, C. E. Bearden, M. Jalbrzikowski, M. Armando, S. Vicari, D. G. Murphy, O. Ousley, L. E. Campbell, T. J. Simon, S. Eliez, International Consortium on Brain and Behavior in 22q11.2 Deletion Syndrome, Psychiatric disorders from childhood to adulthood in 22q11.2 deletion syndrome: Results from the International Consortium on Brain and Behavior in 22q11.2 Deletion Syndrome. *Am. J. Psychiatry* **171**, 627–639 (2014).
19. D. Sun, C. R. K. Ching, A. Lin, J. K. Forsyth, L. Kushan, A. Vajdi, M. Jalbrzikowski, L. Hansen, J. E. Villalon-Reina, X. Qu, R. K. Jonas, T. van Amelsvoort, G. Bakker, W. R. Kates, K. M. Antshel, W. Fremont, L. E. Campbell, K. L. Mc Cabe, E. Daly, M. Gudbrandsen, C. M. Murphy, D. Murphy, M. Craig, J. Vorstman, A. Fiksinski, S. Koops, K. Ruparel, D. R. Roalf, R. E. Gur, J. E. Schmitt, T. J. Simon, N. J. Goodrich-Hunsaker, C. A. Durdle, A. S. Bassett, E. W. C. Chow, N. J. Butcher, F. Vila-Rodriguez, J. Doherty, A. Cunningham, M. B. M. van den Bree, D. E. J. Linden, H. Moss, M. J. Owen, K. C. Murphy, D. M. McDonald-Mc Ginn, B. Emanuel, T. G. M. van Erp, J. A. Turner, P. M. Thompson, C. E. Bearden, Large-scale mapping of cortical alterations in 22q11.2 deletion syndrome: Convergence with idiopathic psychosis and effects of deletion size. *Mol. Psychiatry* **25**, 1822–1834 (2020).
20. D. W. Meechan, T. M. Maynard, E. S. Tucker, A. Fernandez, B. A. Karpinski, L. A. Rothblat, A.-S. LaMantia, Modeling a model: Mouse genetics, 22q11.2 deletion syndrome, and disorders of cortical circuit development. *Prog. Neurobiol.* **130**, 1–28 (2015).
21. L. J. Drew, G. W. Crabtree, S. Markx, K. L. Stark, F. Chaverneff, B. Xu, J. Mukai, K. Fenelon, P.-K. Hsu, J. A. Gogos, M. Karayiorgou, The 22q11.2 microdeletion: Fifteen years of insights into the genetic and neural complexity of psychiatric disorders. *Int. J. Dev. Neurosci.* **29**, 259–281 (2011).
22. E. Scariati, M. Schaer, J. Richiardi, M. Schneider, M. Debbané, D. Van De Ville, S. Eliez, Identifying 22q11.2 deletion syndrome and psychosis using resting-state connectivity patterns. *Brain Topogr.* **27**, 808–821 (2014).
23. C. Schleifer, A. Lin, L. Kushan, J. L. Ji, G. Yang, C. E. Bearden, A. Anticevic, Dissociable disruptions in thalamic and hippocampal resting-state functional connectivity in youth with 22q11.2 deletions. *J. Neurosci.* **39**, 1301–1319 (2019).
24. C. A. Moreau, S. G. W. Urchs, K. Kuldeep, P. Orban, C. Schramm, G. Dumas, A. Labbe, G. Huguet, E. Douard, P. O. Quirion, A. Lin, L. Kushan, S. Grot, D. Luck, A. Mendrek, S. Potvin, E. Stip, T. Bourgeron, A. C. Evans, C. E. Bearden, P. Bellec, S. Jacquemont, Mutations associated with neuropsychiatric conditions delineate functional brain connectivity dimensions contributing to autism and schizophrenia. *Nat. Commun.* **11**, 5272 (2020).
25. C. H. Schleifer, K. P. O'Hora, M. Jalbrzikowski, E. Bondy, L. Kushan-Wells, A. Lin, L. Q. Uddin, C. E. Bearden, Longitudinal development of thalamocortical functional connectivity in 22q11.2 deletion syndrome. *Biol. Psychiatry Cogn. Neurosci. Neuroimaging* **9**, 156–163 (2024).
26. M. Pagani, D. Gutierrez-Barragan, A. E. de Guzman, T. Xu, A. Gozzi, Mapping and comparing fMRI connectivity networks across species. *Commun. Biol.* **6**, 1238 (2023).
27. S. Merscher, B. Funke, J. A. Epstein, J. Heyer, A. Puech, M. M. Lu, R. J. Xavier, M. B. Demay, R. G. Russell, S. Factor, K. Tokooya, B. S. Jore, M. Lopez, R. K. Pandita, M. Lia, D. Carrion, H. Xu, H. Schorle, J. B. Kobler, P. Scambler, A. Wynshaw-Boris, A. I. Skoultchi, B. E. Morrow, R. Kucherlapati, TBX1 is responsible for cardiovascular defects in velo-cardio-facial/DiGeorge syndrome. *Cell* **104**, 619–629 (2001).
28. S. Dutta, P. Sengupta, Men and mice: Relating their ages. *Life Sci.* **152**, 244–248 (2016).
29. A. Liska, A. Galbusera, A. J. Schwarz, A. Gozzi, Functional connectivity hubs of the mouse brain. *Neuroimage* **115**, 281–291 (2015).
30. F. Sforazzini, A. J. Schwarz, A. Galbusera, A. Bifone, A. Gozzi, Distributed BOLD and CBV-weighted resting-state networks in the mouse brain. *Neuroimage* **87**, 403–415 (2014).
31. B. Vogt, G. Paxinos, Cytoarchitecture of mouse and rat cingulate cortex with human homologies. *Brain Struct. Funct.* **219**, 185–192 (2014).
32. N. Brix, A. Ernst, L. L. B. Lauridsen, E. Parner, H. Støvring, J. Olsen, T. B. Henriksen, C. H. Ramlau-Hansen, Timing of puberty in boys and girls: A population-based study. *Paediatr. Perinat. Epidemiol.* **33**, 70–78 (2019).
33. B. T. Yeo, F. M. Krienen, J. Sepulcre, M. R. Sabuncu, D. Lashkari, M. Hollinshead, J. L. Roffman, J. W. Smoller, L. Zollei, J. R. Polimeni, B. Fischl, H. Liu, R. L. Buckner, The organization of the human cerebral cortex estimated by intrinsic functional connectivity. *J. Neurophysiol.* **106**, 1125–1165 (2011).
34. S. N. Wood, *Generalized Additive Models: An Introduction With R* (Chapman and Hall/CRC, 2017).
35. E. Moutin, I. Nikonenko, T. Stefanelli, A. Wirth, E. Ponimaskin, M. De Roo, D. Muller, Palmitoylation of cdc42 promotes spine stabilization and rescues spine density deficit in a mouse model of 22q11.2 deletion syndrome. *Cereb. Cortex* **27**, 3618–3629 (2017).
36. D. Ren, B. Luo, P. Chen, L. Yu, M. Xiong, Z. Fu, T. Zhou, W.-B. Chen, E. Fei, DiGeorge syndrome critical region gene 2 (DGCR2), a schizophrenia risk gene, regulates dendritic spine development through cell adhesion. *Cell Biosci.* **13**, 134 (2023).
37. A.-R. Al-Absi, S. K. Thambiappa, A. R. Khan, S. Glerup, C. Sanchez, A. M. Landau, J. R. Nyengaard, Df (h22q11)/+ mouse model exhibits reduced binding levels of GABAA receptors and structural and functional dysregulation in the inhibitory and excitatory networks of hippocampus. *Mol. Cell. Neurosci.* **122**, 103769 (2022).
38. Y. Zhan, R. C. Paolicelli, F. Sforazzini, L. Weinhard, G. Bolasco, F. Pagani, A. L. Vyssotski, A. Bifone, A. Gozzi, D. Ragozzino, C. T. Gross, Deficient neuron-microglia signaling results in impaired functional brain connectivity and social behavior. *Nat. Neurosci.* **17**, 400–406 (2014).
39. U. Neniskyte, C. T. Gross, Errant gardeners: Glial-cell-dependent synaptic pruning and neurodevelopmental disorders. *Nat. Rev. Neurosci.* **18**, 658–670 (2017).
40. J. Mukai, M. Tamura, K. Fénelon, A. M. Rosen, T. J. Spellman, R. Kang, A. B. MacDermott, M. Karayiorgou, J. A. Gordon, J. A. Gogos, Molecular substrates of altered axonal growth and brain connectivity in a mouse model of schizophrenia. *Neuron* **86**, 680–695 (2015).
41. C. A. Bradley, S. Peineau, C. Taghibiglou, C. S. Nicolas, D. J. Whitcomb, Z. A. Bortolotto, B.-K. Kaang, K. Cho, Y. T. Wang, G. L. Collingridge, A pivotal role of GSK-3 in synaptic plasticity. *Front. Mol. Neurosci.* **5**, 13 (2012).
42. B. Xing, Y.-C. Li, W.-J. Gao, GSK3β hyperactivity during an early critical period impairs prefrontal synaptic plasticity and induces lasting deficits in spine morphology and working memory. *Neuropsychopharmacology* **41**, 3003–3015 (2016).
43. E. Beurel, M. A. Mines, L. Song, R. S. Jope, Glycogen synthase kinase-3 levels and phosphorylation undergo large fluctuations in mouse brain during development. *Bipolar Disord.* **14**, 822–830 (2012).
44. A. McIntosh, F. Bookstein, J. V. Haxby, C. Grady, Spatial pattern analysis of functional brain images using partial least squares. *Neuroimage* **3**, 143–157 (1996).
45. S. Marek, B. Tervo-Clemmens, F. J. Calabro, D. F. Montez, B. P. Kay, A. S. Hatoum, M. R. Donohue, W. Foran, R. L. Miller, T. J. Hendrickson, S. M. Malone, S. Kandala, E. Feczko, O. Miranda-Dominguez, A. M. Graham, E. A. Earl, A. J. Perrone, M. Cordova, O. Doyle, L. A. Moore, G. M. Conan, J. Uriarte, K. Snider, B. J. Lynch, J. C. Wilgenbusch, T. Pengo, A. Tam, J. Chen, D. J. Newbold, A. Zheng, N. A. Seider, A. N. Van, A. Metoki, R. J. Chauvin,

T. O. Laumann, D. J. Greene, S. E. Petersen, H. Garavan, W. K. Thompson, T. E. Nichols, B. T. T. Yeo, D. M. Barch, B. Luna, D. A. Fair, N. U. F. Dosenbach, Reproducible brain-wide association studies require thousands of individuals. *Nature* **603**, 654–660 (2022).
46. L. M. DeVito, H. Eichenbaum, Memory for the order of events in specific sequences: Contributions of the hippocampus and medial prefrontal cortex. *J. Neurosci.* **31**, 3169–3175 (2011).
47. A. Liska, A. Bertero, R. Gomolka, M. Sabbioni, A. Galbusera, N. Barsotti, S. Panzeri, M. L. Scattoni, M. Pasqualetti, A. Gozzi, Homozygous loss of autism-risk gene CNTNAP2 results in reduced local and long-range prefrontal functional connectivity. *Cereb. Cortex* **28**, 1141–1153 (2018).
48. K. J. Gorgolewski, A. Fox, L. Chang, A. Schäfer, K. Arélin, I. Burmann, J. Sacher, D. Margulies, Tight fitting genes: Finding relations between statistical maps and gene expression patterns. *F1000Posters* **5**, 10.7490 (2014).
49. A. M. Buch, P. E. Vértes, J. Seidlitz, S. H. Kim, L. Grosenick, C. Liston, Molecular and network-level mechanisms explaining individual differences in autism spectrum disorder. *Nat. Neurosci.* **26**, 650–663 (2023).
50. F. Koopmans, P. van Nierop, M. Andres-Alonso, A. Byrnes, T. Cijsouw, M. P. Coba, L. N. Cornelisse, R. J. Farrell, H. L. Goldschmidt, D. P. Howrigan, N. K. Hussain, C. Imig, A. P. H. de Jong, H. Jung, M. Kohansalnodehi, B. Kramarz, N. Lipstein, R. C. Lovering, H. MacGillavry, V. Mariano, H. Mi, M. Ninov, D. Osumi-Sutherland, R. Pielot, K. H. Smalla, H. Tang, K. Tashman, R. F. G. Toonen, C. Verpelli, R. Reig-Viader, K. Watanabe, J. van Weering, T. Achsel, G. Ashrafi, N. Asi, T. C. Brown, P. De Camilli, M. Feuermann, R. E. Foulger, P. Gaudet, A. Joglekar, A. Kanellopoulos, R. Malenka, R. A. Nicoll, C. Pulido, J. de Juan-Sanz, M. Sheng, T. C. Südhof, H. U. Tilgner, C. Bagni, À. Bayés, T. Biederer, N. Brose, J. J. E. Chua, D. C. Dieterich, E. D. Gundelfinger, C. Hoogenraad, R. L. Huganir, R. Jahn, P. S. Kaeser, E. Kim, M. R. Kreutz, P. S. McPherson, B. M. Neale, V. O'Connor, D. Posthuma, T. A. Ryan, C. Sala, G. Feng, S. E. Hyman, P. D. Thomas, A. B. Smit, M. Verhage, SynGO: An evidence-based, expert-curated knowledge base for the synapse. *Neuron* **103**, 217–234.e4 (2019).
51. M. J. Gandal, J. R. Haney, B. Wamsley, C. X. Yap, S. Parhami, P. S. Emani, N. Chang, G. T. Chen, G. D. Hoftman, D. de Alba, G. Ramaswami, C. L. Hartl, A. Bhattacharya, C. Luo, T. Jin, D. Wang, R. Kawaguchi, D. Quintero, J. Ou, Y. E. Wu, N. N. Parikshak, V. Swarup, T. G. Belgard, M. Gerstein, B. Pasaniuc, D. H. Geschwind, Broad transcriptomic dysregulation occurs across the cerebral cortex in ASD. *Nature* **611**, 532–539 (2022).
52. M. J. Gandal, P. Zhang, E. Hadjimichael, R. L. Walker, C. Chen, S. Liu, H. Won, H. Van Bakel, M. Varghese, Y. Wang, A. W. Shieh, J. Haney, S. Parhami, J. Belmont, M. Kim, P. M. Losada, Z. Khan, J. Mleczko, Y. Xia, R. Dai, D. Wang, Y. T. Yang, M. Xu, K. Fish, P. R. Hof, J. Warrell, D. Fitzgerald, K. White, A. E. Jaffe, PsychENCODE Consortium, M. A. Peters, M. Gerstein, C. Liu, L. M. Iakoucheva, D. Pinto, D. H. Geschwind, Transcriptome-wide isoform-level dysregulation in ASD, schizophrenia, and bipolar disorder. *Science* **362**, eaat8127 (2018).
53. F. K. Satterstrom, R. K. Walters, T. Singh, E. M. Wigdor, F. Lescai, D. Demontis, J. A. Kosmicki, J. Grove, C. Stevens, J. Bybjerg-Grauholm, M. Bækvad-Hansen, D. S. Palmer, J. B. Maller, iPSYCH-Broad Consortium, M. Nordentoft, O. Mors, E. B. Robinson, D. M. Hougaard, T. M. Werge, P. B. Mortensen, B. M. Neale, A. D. Børglum, M. J. Daly, Autism spectrum disorder and attention deficit hyperactivity disorder have a similar burden of rare protein-truncating variants. *Nat. Neurosci.* **22**, 1961–1965 (2019).
54. F. Delavari, C. Sandini, D. Zöller, V. Mancini, K. Bortolin, M. Schneider, D. Van De Ville, S. Eliez, Dysmaturation observed as altered hippocampal functional connectivity at rest is associated with the emergence of positive psychotic symptoms in patients with 22q11 deletion syndrome. *Biol. Psychiatry* **90**, 58–68 (2021).
55. M. Schreiner, J. K. Forsyth, K. H. Karlsgodt, A. E. Anderson, N. Hirsh, L. Kushan, L. Q. Uddin, L. Mattiacio, I. L. Coman, W. R. Kates, C. E. Bearden, Intrinsic connectivity network-based classification and detection of psychotic symptoms in youth with 22q11.2 deletions. *Cereb. Cortex* **27**, 3294–3306 (2017).
56. M. J. Schreiner, K. H. Karlsgodt, L. Q. Uddin, C. Chow, E. Congdon, M. Jalbrzikowski, C. E. Bearden, Default mode network connectivity and reciprocal social behavior in 22q11.2 deletion syndrome. *Soc. Cogn. Affect. Neurosci.* **9**, 1261–1267 (2014).
57. E. Scariati, M. Schaer, I. Karahanoglu, M. Schneider, J. Richiardi, M. Debbané, D. Van De Ville, S. Eliez, Large-scale functional network reorganization in 22q11.2 deletion syndrome revealed by modularity analysis. *Cortex* **82**, 86–99 (2016).
58. N. Gass, Z. Peterson, J. Reinwald, A. Sartorius, W. Weber-Fahr, M. Sack, J. Chen, H. Cao, M. Didriksen, T. B. Stensbøl, G. Klemme, A. J. Schwarz, E. Schwarz, A. Meyer-Lindenberg, T. Nickl-Jockschat, Differential resting-state patterns across networks are spatially associated with *Comt* and *Trmt2a* gene expression patterns in a mouse model of 22q11.2 deletion. *Neuroimage* **243**, 118520 (2021).
59. J. R. Reinwald, A. Sartorius, W. Weber-Fahr, M. Sack, R. Becker, M. Didriksen, T. B. Stensbøl, A. J. Schwarz, A. Meyer-Lindenberg, N. Gass, Separable neural mechanisms for the pleiotropic association of copy number variants with neuropsychiatric traits. *Transl. Psychiatry* **10**, 93 (2020).
60. J. Mukai, A. Dhilla, L. J. Drew, K. L. Stark, L. Cao, A. B. MacDermott, M. Karayiorgou, J. A. Gogos, Palmitoylation-dependent neurodevelopmental deficits in a mouse model of 22q11 microdeletion. *Nat. Neurosci.* **11**, 1302–1310 (2008).
61. J. D. Power, D. A. Fair, B. L. Schlaggar, S. E. Petersen, The development of human functional brain networks. *Neuron* **67**, 735–748 (2010).
62. V. Menon, Developmental pathways to functional brain networks: Emerging principles. *Trends Cogn. Sci.* **17**, 627–640 (2013).
63. S. Peineau, C. Taghibiglou, C. Bradley, T. P. Wong, L. Liu, J. Lu, E. Lo, D. Wu, E. Saule, T. Bouschet, P. Matthews, J. T. R. Isaac, Z. A. Bortolotto, Y. T. Wang, G. L. Collingridge, LTP inhibits LTD in the hippocampus via regulation of GSK3β. *Neuron* **53**, 703–717 (2007).
64. L. Avrahami, R. Paz, K. Dominko, S. Hecimovic, C. Bucci, H. Eldar-Finkelman, GSK-3-TSC axis governs lysosomal acidification through autophagy and endocytic pathways. *Cell. Signal.* **71**, 109597 (2020).
65. U. Eyo, A. V. Molofsky, Defining microglial-synapse interactions. *Science* **381**, 1155–1156 (2023).
66. A. Mordelt, L. D. de Witte, Microglia-mediated synaptic pruning as a key deficit in neurodevelopmental disorders: Hype or hope? *Curr. Opin. Neurobiol.* **79**, 102674 (2023).
67. J. Koistinaho, T. Malm, G. Goldsteins, Glycogen synthase kinase-3β: A mediator of inflammation in Alzheimer's disease? *Int. J. Alzheimers Dis.* **2011**, 129753 (2011).
68. L. Q. Uddin, K. Supekar, V. Menon, Reconceptualizing functional brain connectivity in autism from a developmental perspective. *Front. Hum. Neurosci.* **7**, 458 (2013).
69. B. Chen, A. Linke, L. Olson, C. Ibarra, S. Reynolds, R.-A. Müller, M. Kinnear, I. Fishman, Greater functional connectivity between sensory networks is related to symptom severity in toddlers with autism spectrum disorder. *J. Child Psychol. Psychiatry* **62**, 160–170 (2021).
70. R. Jalal, A. Nair, A. Lin, A. Eckfeld, L. Kushan, J. Zinberg, K. H. Karlsgodt, T. D. Cannon, C. E. Bearden, Social cognition in 22q11.2 deletion syndrome and idiopathic developmental neuropsychiatric disorders. *J. Neurodev. Disord.* **13**, 15 (2021).
71. B. Milic, C. Feller, M. Schneider, M. Debbané, H. Loeffler-Stastka, Social cognition in individuals with 22q11.2 deletion syndrome and its link with psychopathology and social outcomes: A review. *BMC Psychiatry* **21**, 130 (2021).
72. T. Matsuo, T. Hattori, A. Asaba, N. Inoue, N. Kanomata, T. Kikusui, R. Kobayakawa, K. Kobayakawa, Genetic dissection of pheromone processing reveals main olfactory system-mediated social behaviors in mice. *Proc. Natl. Acad. Sci. U.S.A.* **112**, E311–E320 (2015).
73. A. Senju, M. H. Johnson, The eye contact effect: Mechanisms and development. *Trends Cogn. Sci.* **13**, 127–134 (2009).
74. A. Tripathi, M. Spedding, E. Schenker, M. Didriksen, A. Cressant, T. M. Jay, Cognition-and circuit-based dysfunction in a mouse model of 22q11.2 microdeletion syndrome: Effects of stress. *Transl. Psychiatry* **10**, 41 (2020).
75. J. Maeder, C. Sandini, D. Zöller, M. Schneider, M. Bostelmann, V. Pouillard, P. Caroni, M. Kliegel, S. Eliez, Long-term verbal memory deficit and associated hippocampal alterations in 22q11.2 deletion syndrome. *Child Neuropsychol.* **26**, 289–311 (2020).
76. M. Tamura, J. Mukai, J. A. Gordon, J. A. Gogos, Developmental inhibition of Gsk3 rescues behavioral and neurophysiological deficits in a mouse model of schizophrenia predisposition. *Neuron* **89**, 1100–1109 (2016).
77. G. P. Meares, R. S. Jope, Resolution of the nuclear localization mechanism of glycogen synthase kinase-3: Functional effects in apoptosis. *J. Biol. Chem.* **282**, 16989–17001 (2007).
78. D. Wu, W. Pan, GSK3: A multifaceted kinase in Wnt signaling. *Trends Biochem. Sci.* **35**, 161–168 (2010).
79. C.-W. Woo, A. Krishnan, T. D. Wager, Cluster-extent based thresholding in fMRI analyses: Pitfalls and recommendations. *Neuroimage* **91**, 412–419 (2014).
80. M. Allen, D. Poggiali, K. Whitaker, T. R. Marshall, J. van Langen, R. A. Kievit, Raincloud plots: A multi-platform tool for robust data visualization. *Wellcome Open Res.* **4**, 10.12688/wellcomeopenres.15191.2 (2019).
81. H. Huang, C. Michetti, M. Busnelli, F. Manago, S. Sannino, D. Scheggia, L. Giancardo, D. Sona, V. Murino, B. Chini, M. L. Scattoni, F. Papaleo, Chronic and acute intranasal oxytocin produce divergent social effects in mice. *Neuropsychopharmacology* **39**, 1102–1114 (2014).
82. L. W. Hung, S. Neuner, J. S. Polepalli, K. T. Beier, M. Wright, J. J. Walsh, E. M. Lewis, L. Luo, K. Deisseroth, G. Dölen, R. C. Malenka, Gating of social reward by oxytocin in the ventral tegmental area. *Science* **357**, 1406–1411 (2017).
83. B. L. Pearson, J. K. Bettis, K. Z. Meyza, L. Y. Yamamoto, D. C. Blanchard, R. J. Blanchard, Absence of social conditioned place preference in BTBR T+ tf/J mice: Relevance for social motivation testing in rodent models of autism. *Behav. Brain Res.* **233**, 99–104 (2012).
84. M. Yang, J. L. Silverman, J. N. Crawley, Automated three-chambered social approach task for mice. *Curr. Protoc. Neurosci.* **56**, 8.26.1–8.26.16 (2011).
85. F. Papaleo, F. Yang, C. Paterson, S. Palumbo, G. V. Carr, Y. Wang, K. Floyd, W. Huang, C. J. Thomas, J. Chen, D. R. Weinberger, A. J. Law, Behavioral, neurophysiological, and synaptic impairment in a transgenic neuregulin1 (NRG1-IV) murine schizophrenia model. *J. Neurosci.* **36**, 4859–4875 (2016).
86. V. Kebets, P. Favre, J. Houenou, M. Polosan, N. Perroud, J.-M. Aubry, D. Van De Ville, C. Piguet, Fronto-limbic neural variability as a transdiagnostic correlate of emotion dysregulation. *Transl. Psychiatry* **11**, 545 (2021).

87. E. C. Walvoord, The timing of puberty: Is it changing? Does it matter? *J. Adolesc. Health* **47**, 433–439 (2010).
88. R. M. Ghandour, L. J. Sherman, C. J. Vladutiu, M. M. Ali, S. E. Lynch, R. H. Bitsko, S. J. Blumberg, Prevalence and treatment of depression, anxiety, and conduct problems in US children. *J. Pediatr.* **206**, 256–267.e3 (2019).
89. K. Sayal, V. Prasad, D. Daley, T. Ford, D. Coghill, ADHD in children and young people: Prevalence, care pathways, and service provision. *Lancet Psychiatry* **5**, 175–186 (2018).
90. J. N. Constantino, C. P. Gruber, *Social Responsiveness Scale* (Western Psychological Services, ed. 2, 2012).
91. D. Wechsler, *Wechsler Abbreviated Scale of Intelligence (WASI--II)* (NCS Pearson, ed. 2, 2011).
92. M. First, R. Spitzer, J. Williams, *Structured Clinical Interview for DSM-IV Axis I Disorders Clinician Version SCID-I. Developmental Disorder Addition* (American Psychiatric Association, 2009).
93. T. H. McGlashan, T. J. Miller, S. W. Woods, R. E. Hoffman, L. Davidson, "Instrument for the assessment of prodromal symptoms and states" in *Early Intervention in Psychotic Disorders*, T. Miller, S. A. Mednick, T. H. McGlashan, J. Libiger, J. O. Johannessen, Eds. (Springer, 2001), pp. 135–149.
94. C. Lord, S. Risi, L. Lambrecht, E. H. Cook Jr., B. L. Leventhal, P. C. DiLavore, A. Pickles, M. Rutter, The autism diagnostic observation schedule—Generic: A standard measure of social and communication deficits associated with the spectrum of autism. *J. Autism Dev. Disord.* **30**, 205–223 (2000).
95. M. Jalbrzikowski, K. H. Ahmed, A. Patel, R. Jonas, L. Kushan, C. Chow, C. E. Bearden, Categorical versus dimensional approaches to autism-associated intermediate phenotypes in 22q11.2 microdeletion syndrome. *Biol. Psychiatry Cogn. Neurosci. Neuroimaging* **2**, 53–65 (2017).
96. C. Craddock, S. Sikka, B. Cheung, R. Khanuja, S. S. Ghosh, C. Yan, Q. Li, D. Lurie, J. Vogelstein, R. Burns, S. Colcombe, M. Mennes, C. Kelly, A. Di Martino, F. X. Castellanos, M. Milham, Towards automated analysis of connectomes: The configurable pipeline for the analysis of connectomes (c-pac). *Front. Neuroinform.* **42**, 10.3389/conf.fninf.2013.09.00042 (2013).
97. J.-P. Fortin, N. Cullen, Y. I. Sheline, W. D. Taylor, I. Aselcioglu, P. A. Cook, P. Adams, C. Cooper, M. Fava, P. J. McGrath, M. McInnis, M. L. Phillips, M. H. Trivedi, M. M. Weissman, R. T. Shinohara, Harmonization of cortical thickness measurements across scanners and sites. *Neuroimage* **167**, 104–120 (2018).
98. K. J. Gorgolewski, G. Varoquaux, G. Rivera, Y. Schwarz, S. S. Ghosh, C. Maumet, V. V. Sochat, T. E. Nichols, R. A. Poldrack, J.-B. Poline, T. Yarkoni, D. S. Margulies, NeuroVault.Org: A web-based repository for collecting and sharing unthresholded statistical maps of the human brain. *Front. Neuroinform.* **9**, 8 (2015).
99. D. Szklarczyk, A. L. Gable, D. Lyon, A. Junge, S. Wyder, J. Huerta-Cepas, M. Simonovic, N. T. Doncheva, J. H. Morris, P. Bork, L. J. Jensen, C. Von Mering, STRING v11: Protein–protein association networks with increased coverage, supporting functional discovery in genome-wide experimental datasets. *Nucleic Acids Res.* **47**, D607–D613 (2019).
100. F. K. Satterstrom, J. A. Kosmicki, J. Wang, M. S. Breen, S. De Rubeis, J.-Y. An, M. Peng, R. Collins, J. Grove, L. Klei, C. Stevens, J. Reichert, M. S. Mulhern, M. Artomov, S. Gerges, B. Sheppard, X. Xu, A. Bhaduri, U. Norman, H. Brand, G. Schwartz, R. Nguyen, E. E. Guerrero, C. Dias, Autism Sequencing Consortium, iPSYCH-Broad Consortium, C. Betancur, E. H. Cook, L. Gallagher, M. Gill, J. S. Sutcliffe, A. Thurm, M. E. Zwick, A. D. Børglum, M. W. State, A. E. Cicek, M. E. Talkowski, D. J. Cutler, B. Devlin, S. J. Sanders, K. Roeder, M. J. Daly, J. D. Buxbaum, Large-scale exome sequencing study implicates both developmental and functional changes in the neurobiology of autism. *Cell* **180**, 568–584.E23 (2020).
101. J. Grove, S. Ripke, T. D. Als, M. Mattheisen, R. K. Walters, H. Won, J. Pallesen, E. Agerbo, O. A. Andreassen, R. Anney, S. Awashti, R. Belliveau, F. Bettella, J. D. Buxbaum, J. Bybjerg-Grauholm, M. Bækvad-Hansen, F. Cerrato, K. Chambert, J. H. Christensen, C. Churchhouse, K. Dellenvall, D. Demontis, S. De Rubeis, B. Devlin, S. Djurovic, A. L. Dumont, J. I. Goldstein, C. S. Hansen, M. E. Hauberg, M. V. Hollegaard, S. Hope, D. P. Howrigan, H. Huang, C. M. Hultman, L. Klei, J. Maller, J. Martin, A. R. Martin, J. L. Moran, M. Nyegaard, T. Nærland, D. S. Palmer, A. Palotie, C. B. Pedersen, M. G. Pedersen, T. dPoterba, J. B. Poulsen, B. S. Pourcain, P. Qvist, K. Rehnström, A. Reichenberg, J. Reichert, E. B. Robinson, K. Roeder, P. Roussos, E. Saemundsen, S. Sandin, F. K. Satterstrom, G. D. Smith, H. Stefansson, S. Steinberg, C. R. Stevens, P. F. Sullivan, P. Turley, G. B. Walters, X. Xu, Autism Spectrum Disorder Working Group of the Psychiatric Genomics Consortium, BUPGEN, Major Depressive Disorder Working Group of the Psychiatric Genomics Consortium, 23andMe Research Team, K. Stefansson, D. H. Geschwind, M. Nordentoft, D. M. Hougaard, T. Werge, O. Mors, P. B. Mortensen, B. M. Neale, M. J. Daly, A. D. Børglum, Identification of common genetic risk variants for autism spectrum disorder. *Nat. Genet.* **51**, 431–444 (2019).
102. J. B. Burt, M. Helmer, M. Shinn, A. Anticevic, J. D. Murray, Generative modeling of brain maps with spatial autocorrelation. *Neuroimage* **220**, 117038 (2020).

Acknowledgments: We would like to dedicate this work to the cherished memory of Andrea Baracchino. **Funding:** This work was supported by a MCHRI Uytengsu-Hamilton 22q11 Neuropsychiatry Research Award (UH22QEXTFY22-04 to A.G. and C.E.B.), the NIH (1R21MH116473-01A1 to A.G. and C.E.B. and R37MH085953 to C.E.B.), and the European Research Council (ERC; DISCONN, no. 802371 to A.G.). A.G. was also supported by the Brain and Behavior Foundation 2017 [National Alliance for Research on Schizophrenia and Depression (NARSAD)], the Telethon foundation (GGP19177), and by an endowment by P. Baracchino and S. Baracchino. M.P. was supported by the European Union's Horizon 2020 research and innovation program under grant agreement no. 845065 (Marie Sklodowska-Curie Global Fellowship - CANSAS). M.V.L. acknowledges funding by the ERC under the European Union's Horizon 2020 research and innovation program under grant agreement no. 755816. M.P. was supported by the EU H2020 MSCA ITN Project "Serotonin and Beyond" (no. 953327); the Next Generation EU National Recovery and Resilience Plan and Ministry of University and Research (no. ECS 00000017 "Tuscany Health Ecosystem THE," Spoke 8); MIUR, Grant of the Department of Excellence 2023–2027; and MIUR PRIN 2022 PNRR (P2022ZEMZF). D.M. was supported by Innovative Medicines Initiative 2 Joint Undertaking for the project EU-AIMS (grant no. 115300) and for the project AIMS-2-TRIALS (grant no. 777394). W.R.K. was supported by the National Institute of Mental Health under grant nos. MH64824 and MH65481. **Author contributions:** Conceptualization: A.Go., C.E.B., and D.M. Methodology: F.G.A., S.G., M.Pag., C.S., E.D.G., C.M., N.B., F.P., C.E.B., and A.Go. Formal analysis: F.G.A., S.G., D.S.-Y., A.M., and A.Go. Investigation: F.G.A., S.G., A.Ga., A.M., D.S.-Y., C.S., L.K., A.S., W.R.K., M.Pas., C.EB., and A.Go. Visualization: A.Go., F.G.A., S.G., C.E.B., M.Pas., and A.M. Supervision: A.Go., C.E.B., M.Pas., and M.V.L. Writing—original draft: A.Go., F.G.A., S.G., C.E.B., and M.V.L. Writing—review and editing: A.Go., F.G.A., S.G., C.S., L.K., C.E.B., A.M., M.V.L., and D.M. Software: S.G. and A.Go. Funding acquisition: A.Go., C.E.B., M.Pas., and D.M. Resources: A.Ga., F.P., C.E.B., A.Go., D.M., and A.S. Validation: A.M., A.Ga., C.E.B., A.Go., and D.M. Data curation: A.M., C.S., L.K., C.B., A.Go., and D.M. Project administration: A.Go., C.E.B., and D.M. **Competing interests:** D.M. has received payment from Springer for editorial duties and has served on an advisory board for Roche. The other authors declare that they have no competing interests. **Data and materials availability:** Raw and preprocessed mouse and human fMRI data, respectively, are available at https://doi.org/10.5281/zenodo.14534419 (juvenile mice data), https://doi.org/10.5281/zenodo.14534751 (adult mice data), and https://doi.org/10.5281/zenodo.14639219 (human data). Configuration file for the preprocessing of human fMRI data is available at https://doi.org/10.5281/zenodo.14761241. Additionally, human behavioral data are available at https://nda.nih.gov/edit_collection.html?id=2414. The code used for preprocessing mouse fMRI data is available at https://doi.org/10.5281/zenodo.10218169. Code for calculating global connectivity in mice and humans is available at https://doi.org/10.5281/zenodo.10218258. Code for calculating seed-based mapping in mice and humans is available at https://doi.org/10.5281/zenodo.10218158. Code for gene enrichment analysis is available at https://doi.org/10.5281/zenodo.13991845. Functional connectivity quantifications were plotted using R and the raincloud plots library (*80*). Glass brain visualization for human data was plotted using the corresponding nilearn function. Participants' icons and arrows are from Microsoft PowerPoint (2021). All data needed to evaluate the conclusions in the paper are present in the paper and/or the Supplementary Materials.

Submitted 8 May 2024
Accepted 4 February 2025
Published 12 March 2025
10.1126/sciadv.adq2807